SOLUBILITIES OF CO AND H_2 IN NEAT AND CO_2-EXPANDED HYDROFORMYLATION REACTION MIXTURES CONTAINING 1-OCTENE AND NONANAL UP TO 80 °C AND 90 BARS

BY

Zhuanzhuan Xie

B.S. Chemical Engineering, Tianjin University, 2006

Submitted to the graduate degree program in Chemical & Petroleum Engineering and the Graduate Faculty of the University of Kansas School of Engineering in partial fulfillment of the requirements for the degree of Master of Science

Chairperson: Bala Subramaniam

Committee members* Raghunath V. Chaudhari *

Aaron M. Scurto *

Date defended: 12/11/2008

The Thesis Committee for Zhuanzhuan Xie certifies
that this is the approved version of the following thesis:

SOLUBILITIES OF CO AND H_2 IN NEAT AND CO_2-EXPANDED HYDROFORMYLATION REACTION MIXTURES CONTAINING 1-OCTENE AND NONANAL UP TO 80 °C AND 90 BARS

Committee:

_____
Chairperson* Bala Subramaniam

_____
Raghunath V. Chaudhari

_____
Aaron M. Scurto

Date approved_____

ABSTRACT

Accurate knowledge of the phase equilibria of CO_2-expanded hydroformylation reaction mixtures is essential to rational process design and development. Vapor liquid equilibria of the following systems were measured in a variable volume view cell at temperatures ranging from 40 °C to 80 °C and pressures up to 90 bars: CO/1-octene, CO_2/1-octene, CO/1-octene/CO_2, CO/nonanal, CO_2/nonanal, CO/nonanal/CO_2, H_2/1-octene, H_2/1-octene/CO_2, H_2/nonanal and H_2/nonanal/CO_2. The measured solubilities of CO and H_2 in the liquid phases were consistent with literature values. The presence of CO_2 was found to enhance the solubilities of both CO and H_2 in the liquid phase. The enhancement factor is up to 1.54 for carbon monoxide and 1.82 for hydrogen. The Peng-Robinson equation of state (PR EoS) with van der Waals mixing rules and binary interaction parameters modeled the VLE data adequately, with much better fits for the 1-octene systems compared to the more polar nonanal systems.

DEDICATED TO

My Family

ACKNOWLEDGEMENTS

To my advisor, Professor Bala Subramaniam, for his patience and encouragement when I had a hard time in my research, also for his feedback and guidance to my work.

To my committee members, Professor Raghunath Vitthal Chaudhari and Professor Aaron Scurto for their critical evaluations and inputs in my research work.

To Dr. William Kirk Snavely, for his assistance and guidance in building up the experimental apparatus and developing the analytical method for this work.

To Ed Atchison and Alan Walker, for their kind assistance in instrumentation.

To Chad Johnson, Jing Fang, Kening Gong, Dr. Shengwei Tang, Dr. Jackson Ford, Madhav Ghanta, Meng Li and Wei Ren for the wonderful experiences of collaborations.

To my parents, my brother and my boyfriend, for their love and support.

To my sources of funding, National Science Foundation.

TABLE OF CONTENTS

LIST OF FIGURES

LIST OF TABLES

CHAPTER 1 INTRODUCTION AND LITERATURE REVIEW

1.1 CO_2-expanded Hydroformylation Process

Hydroformylation is an important industrial process for the production of aldehydes from alkenes using synthesis gas or "syngas", a mixture of H_2 and CO as reagent [Roelen, 1938/1952]. This chemical reaction entails the addition of a formyl group (CHO) and a hydrogen atom to a carbon-carbon double bond.

The formula of the raction is as follows:

$$RCH=CH_2+H_2+CO \xrightarrow{Catalyst} RCH_2CH_2CHO(n)+RCH(CH_3)CHO(i)+InternalAldehydes$$

The reaction produces linear (*n*-), branched (*iso or i*-) as well as internal aldehydes, which are further hydrogenated or oxidized to corresponding alcohols and acids. The reaction is mostly accomplished with a rhodium- or cobalt-based catalyst.

Hydroformylation reaction is important because the resulting aldehydes are easily converted into many secondary products. The main products are used for the production of alcohols, carboxylic acids, aldol products, diols, acetals, ethers, acroleins and esters [Trzeciak and Ziółkowski, 1999]. In commodity chemical industry, linear aldehydes or high *n/i* molar ratios (>5) are preferred for producing plasticizers, detergents, and solvents [Leeuwen and Claver, 2000; Cornils and Herrmann, 2002]. For specialty chemicals and pharmaceuticals, however, branched aldehydes are often desired. Specifically, the hydroformylation of 1-octene is performed in the production of plasticizer alcohols and biodegradable detergents.

Recently, one of the challenges in hydroformylation research is searching for novel temperature or pressure-tunable solvent media which makes it possible to

conduct reactions in a homogeneous manner and catalyst recovery through phase separation without changing the composition of the reaction mixture. The use of a new class of solvents, CO_2-expanded liquids (CXLs) as reaction media has received increased attention. CXLs are a promising alternative for performing olefin hydroformylation under mild conditions. A CXL is a mixture composed of subcritical CO_2 condensed into an organic solvent. By varying the CO_2 composition, a continuum of liquid media ranging from the neat organic solvent to compressed CO_2 is generated, the properties of which can be adjusted by tuning the operating pressure: a large amount of CO_2 favors gas solubility and the presence of polar organic solvents enhances metal catalyst solubility. Further, higher CO_2 composition leads to lower dielectric constant of the solvent media and reduced catalyst solubility, or even causes catalysts to precipitate from the expanded liquid phase (antisolvent effect), suggesting that CXLs may also be used for catalyst recovery.

CXLs have been shown to be optimal solvents in a variety of roles inducing separations, precipitating fine particles, facilitating polymer processing, and serving as reaction media for catalytic reactions [Jessop and Subramaniam, 2007]. Process advantages include ease of removal of the CO_2, enhanced solubility of reagent gases (compared to liquid solvents), fire suppression capability of the CO_2, and milder process pressures (tens of bars) compared to *sc*CO_2 (hundreds of bars). Reaction advantages include higher gas miscibility compared to organic solvents at ambient conditions, enhanced transport rates due to the properties of dense CO_2, and between 1 and 2 orders of magnitude greater rates than in neat organic. Environmental

advantages include substantial replacement of organic solvents with environmentally benign dense-phase CO_2. Thus, CXLs have emerged as important components in the optimization of chemical processes.

CXLs are optimal reaction media for catalytic hydroformylation reactions. The presence of CO_2 improved the syngas availability in the liquid phase and enhanced the selectivity to the desired aldehyde products. Studies at two temperatures, 30 and 60 °C, showed more than a fourfold increase in the aldehyde yields in CO_2-expanded acetone, when compared to both neat acetone and neat CO_2 as solvents [Jin et al., 2006]. This increase is attributed to the favorable syngas solubility and dielectric constant in CXLs compared to neat organic solvent and neat CO_2, respectively. Reduction in temperature favored hydroformylation reaction and suppressed byproducts from the hydrogenation and isomerization of the olefin substrate. Increase in H_2 concentration led to improved hydroformylation rates.

1.2 Phase Equilibria Involving CXLs

As CO_2 dissolves into an organic liquid, the liquid expands volumetrically, forming a CXL. Not all liquids expand equally in the presence of CO_2 pressure, and the differences in behavior are attributed to differences in the ability of the liquids to dissolve CO_2. In this regard, liquids can be divided into three general classes [Heldebrant et al., 2006], and there is variation within the classes. Class I liquids such as water have insufficient ability to dissolve CO_2 and, therefore, do not expand significantly and have essentially no change in their properties, except acidity. Class

II liquids, such as methanol, hexane, and most other traditional organic solvents, dissolve large amounts of CO_2, expand greatly, and consequently undergo significant changes in virtually every physical property. Class III liquids, such as liquid polymers and crude oil, dissolve only moderate amounts of CO_2 and, therefore, expand only moderately in volume. As a result, some properties such as viscosity change significantly while others, such as polarity, do not.

Accurate knowledge of phase equilibria of hydroformylation reactions in CO_2-expanded liquid is essential to process design and development. It helps to determine optimal operating conditions for maximizing the yield of the desired product. It also benefits molecular dynamics simulations. Other uses for phase equilibrium data include the simulation of petroleum reservoirs, enhanced oil recovery, the transportation and storage of natural gas, and the study of geological processes.

Information about experimental equilibrium data is important, even when thermodynamic models are used to calculate the phase behavior of a mixture. Thermodynamic models can help to reduce the number of experimental data points needed for a special design problem. But very often, at least some experimental data points are needed to obtain reliable interaction parameters for the model [Dohrn et al., 1994].

There are many ways to obtain information about the phase behavior of fluid mixtures. Experimental methods for the investigation of high-pressure phase equilibria can be divided into two classes, depending on how the composition is determined: analytical methods (or direct sampling methods) and synthetic methods

(or indirect methods) [Christov and Dohrn, 2002].

Analytical methods involve the determination of the compositions of the coexisting phases. This can be done by taking samples from each phase and analyzing them outside the equilibrium cell at normal pressure or by using physicochemical methods of analysis inside the equilibrium cell under pressure, e.g. spectroscopic methods. Depending on the attainment of equilibrium, analytical methods can be classified as isothermal methods, isobaric-isothermal methods and isobaric methods.

The idea behind synthetic methods is to prepare a mixture of known composition and then observe the phase behavior in an equilibrium cell. No sampling is necessary. The problem of analyzing fluid mixtures is replaced by the problem of "synthesizing" them. After known amounts of the components are placed into an equilibrium cell, values of temperature and pressure are adjusted so that the mixture is homogeneous. Then the temperature or pressure is varied until the formation of a new phase is observed. Each experiment yields one point of the P-T-x phase envelope.

When phase separation is difficult due to similar densities of the coexisting phases, e.g. near or even at critical points and in barotropic systems, where at certain conditions the coexisting phases have the same density, synthetic methods are generally used. For multi-component systems, experiments with synthetic methods yield less information than with analytical methods, because the tie lines cannot be determined without additional experiments. Therefore, synthetic methods are rarely used for ternary systems. Since the systems investigated in this work are mainly ternary or even quaternary systems, isobaric-isothermal analytical method is used.

1.3 Permanent Gas Solubilities in CXLs: Objective of the Present Work

A large number of publications may be found on the vapor-liquid equilibrium of CO (or H_2) + organic liquid and CO (or H_2) + CO_2 binary systems. Katayama *et al.* [1975] reported the isothermal vapor-liquid equilibrium data for the acetone/CO_2 systems at 25 °C (13 pressures, 4-61 atm) and 40 °C (12 pressures, 10-73 atm), and for the methanol/CO_2 system at 25 °C (13 pressures, 2-60 atm). Brunner [1985] reported H_2 solubility measurements in ten organic solvents (including acetone) at 25, 50, and 100 ºC and pressures up to 10 MPa. Purwanto *et al*. [1996] measured the solubilities of H_2 and CO in 1-octene, acetone, acetonitrile, water, and ethanol at 25 and 50 °C. Jáuregui-Haza *et al.* [2004] reported the solubility measurements of H_2 and CO in water, octane, toluene and nonanal at 353 K, 363 K, 373 K in a pressure range of 0.5-1.5 MPa. Jacquemin *et al.* [2006] measured the solubility of carbon dioxide, ethane, methane, oxygen, nitrogen, hydrogen, argon, and carbon monoxide in 1-butyl-3-methylimidazolium tetrafluoroborate between temperatures 283K and 343K and at pressures close to atmospheric. Still *et al.* [2006] measured the solubilities of 1-butene, carbon monoxide and hydrogen in the 2,2,4-trimethyl-1,3-pentanediol mono(2-methylpropanoate) solvent (NX 795) at a partial pressure of 101.3 kPa and a temperature range from 273 to 373 K. Deschamps *et al*. [2007] presented the solubility of O_2, CO_2, CO in three fluorinated liquids - perfluorohexylethane, perfluorooctane and bromoperfluorooctane at temperature between (288 and 313) K. Kumelan *et al.* [2007] measured the solubility of the single gases hydrogen and carbon monoxide in the ionic liquid 1-n-butyl-3-

methylimidazolium methyl sulfate ([bmim][CH_3SO_4]) with a high-pressure view-cell technique based on the synthetic method. The temperature ranged from 293 to 413 K, and the pressure reached up to 9.3 MPa. Solubilities of carbon monoxide and hydrogen in propylene carbonate (PC), biphasic mixture of PC and dodecane (1:1 v/v) and thermomorphic (or temperature dependent) multicomponent solvent (TMS)-system consisting of PC, dodecane and 1,4-dioxane were measured over the temperature and pressure range of 298–343K and 0.1–1.5MPa by Shaharun *et al*. [2008].

Kaminishi *et al.* [1968] and Christiansen *et al.* [1974] reported the solubility of CO in liquid CO_2 at 10 °C. Christov and Dohrn [2002] published a comprehensive review summarizing various high-pressure fluid phase equilibria for many gas (including CO_2, H_2, or CO) + organic liquid binary systems. In the range of temperatures and pressures reported in these referenced studies, the CO and H_2 solubilities in the liquid phase follow Henry's law.

In contrast, relatively few publications were found dealing with CO (and/or H_2) + CO_2 + organic liquid ternary and quaternary systems. The emerging interest in CXLs as solvent media for catalytic reactions, especially those involving gaseous reactants (such as in hydrogenation, oxidation, carbonylation, and hydroformylation), has led to increased research into the phase equilibria of (gas + CO_2 + organic/inorganic liquid) type systems. Bezanehtak *et al.* [2004] investigated the vapor-liquid equilibria for the CO_2 + H_2 + methanol ternary system at temperatures of 5, 15 and 25 °C and pressures up to 20 MPa. Solinas *et al.* [2004] measured the concentrations of H_2 in the

CO_2/ionic liquid (IL) media at room temperature using an *in-situ* NMR 44 probe. Hert *et al.* [2005] reported the solubilities of O_2 and CH_4 in CO_2 + 1-hexyl-3-methylimidazolium bis(trifluoromethylsulfonyl) imide ([hmim][Tf_2N]) media at 25 °C with various CO_2 feed compositions. Xie *et al.* [2005] measured the bubble/dew points for H_2 + CO_2 + methanol system with various CO_2 compositions at 40 °C. Yin and Tan [2006] reported their study on the solubility of H_2 in liquid toluene in the presence of compressed CO_2 at the temperatures from 305 to 343 K and the pressures from 1.2 to 10.5 MPa by using a continuous flow technique. Lopez-Castillo *et al.* [2006] reported the solubility of O_2 and CO in CO_2-expanded acetonitrile, acetone, and methanol at temperatures between 25 and 40 °C and pressures to 90 bar. Zevnik *et al.* [2007] measured hydrogen solubility in CO_2-expanded 2-propanol and in propane-expanded 2-propanol at 298 K and partial pressure of H_2 up to 6 MPa and 333 K and partial pressure of H_2 up to 5 MPa separately. Lopez-Castillo *et al.* [2008] reported the Vapor-liquid equilibrium (VLE) data for the systems CO_2/H_2/acetonitrile, CO_2/H_2/acetone, and CO_2/H_2/methanol were determined at 40 °C and 25, 60, and 90 bar. Up to now, the solubility studies in CO_2-expanded liquids are still very limited and system-specific in nature. Houndonougbo *et al*. [2006, 2007] used Monte Carto and molecular dynamics to simulate the phase equilibria and transport properties in carbon-dioxide expanded acetonitrile, methanol, ethanol, acetone, acetic acid, toluene, and 1-octene. Guha *et al.* [2007] showed a detailed reactor model incorporating reaction kinetics, mass transfer rates and phase equilibrium to systematically investigate the effects of mass transfer and catalyst activation on induction period in

1-octene hydroformylation in CXL. Extensive experimental measurements, combined with modeling studies using empirical equation of states or molecular simulation methods, are not only important to gain a better fundamental understanding of the continuum of CXL media, but also to their rational application in many multi-phase catalytic processes.

Concentrations of H_2 and CO affect the reaction rates in different ways. Accurate CO and H_2 activity data in CXLs are necessary for reliable interpretation of conversion/selectivity data. The objectives of this work are to:

Measure the intrinsic solubility of syngas (CO and H_2) in the continuum of CO_2-expanded hydroformylation reactants and products (1-octene and nonanal) under pressures and temperatures encountered in homogeneous catalytic hydroformylation (up to 80 °C, 80 bars);

Develop thermodynamic models to describe vapor-liquid equilibria of the binary and ternary systems using the binary interaction parameters to predict the multi-component system phase equilibria.

Successful pursuit of these objectives will help in the reliable modeling of hydroformylation reactors and catalyst separations that employ CXLs as reaction media [Subramaniam et al., 2008].

CHAPTER 2 EXPERIMENTAL EQUIPMENT AND PROCEDURES FOR PHASE BEHAVIOR STUDIES

2.1 Introduction

A variable volume cell was suitably modified to ensure adequate mixing of the liquid and vapor phases before sampling for analysis. Gas Chromatography (GC) is used in this work to determine the compositions of the liquid and vapor phases at equilibrium. The equipment modifications and the analytical procedures for quantitative analyses of the various components are described in detail in this chapter.

2.2 Phase Equilibrium Apparatus

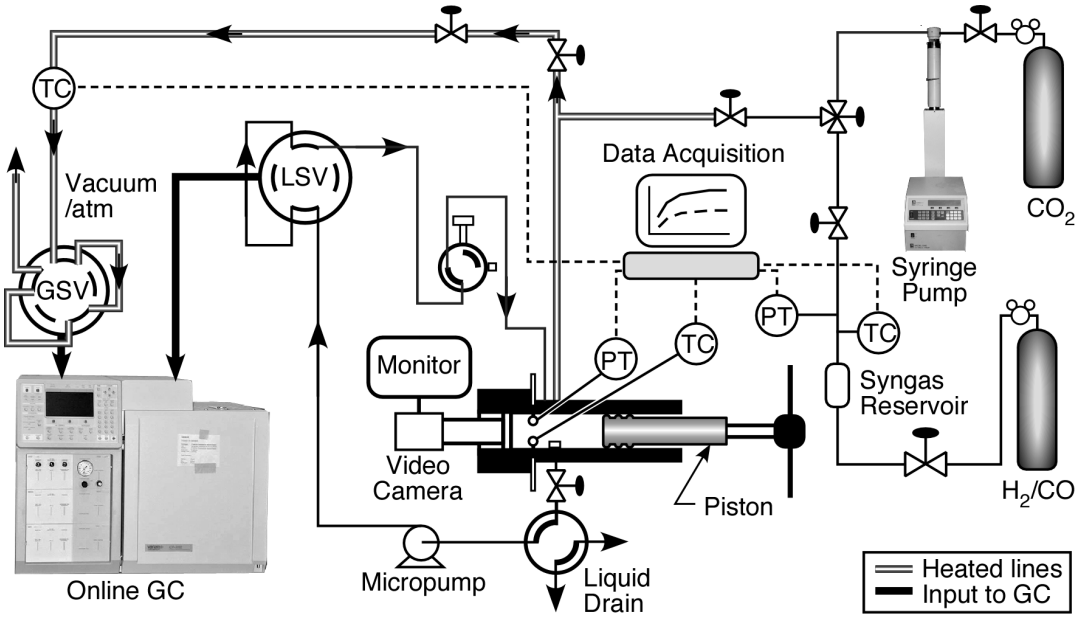

Figure 2.1: Apparatus for solubility measurements

The apparatus (Figure 2.1) for measuring solubility of hydrogen and carbon monoxide in CO_2-expanded 1-octene/nonanal mixtures consists of a SFT phase monitor II (Supercritical Fluid Technologies, Inc.), two Valco® four-port valves

(Valco Instruments Co. Inc), a Micropump® (IDEX corporation), a syringe pump (Model 500D, Teledyne Isco, Inc.) and the liquid and gas sampling valves (Valco Instruments Co. Inc) in the GC (Varian CP-3800), and a Camile® 3300 data acquisition and control system.

The SFT Phase Monitor II consists of a manually controlled syringe pump integrated within a 30 ml view cell. The volume of the view cell can be varied from 3 ml to 30 ml. A CCD camera with a fiber optic light source allows clear viewing of the cell's interior. The image is displayed on the TV/VCR monitor. The view cell can be oriented in a horizontal position for solubility work with liquid materials and in a vertical configuration for solubility work with solid materials. The sample holder accommodates liquid, solid and powder samples. Fluid mixing is achieved through rare earth magnets coupled to an internally mounted impeller as well as the circulation of the fluid. An internal Resistance Temperature Detector (RTD) is used to measure the temperature. A fuzzy logic controller (AI-100, Total Temperature Instrumentation, Inc.) uniformly controls the heating of the view cell up to 150 °C with an uncertainty of ± 0.5 °C. The pressure gauge is composed of a pressure transducer and an Analog Input Panel Meter (Red Lion Controls, Inc.) with an uncertainty of ± 13.8 kPa in pressures ranging from vacuum to 20 MPa. Figure 2.2 shows an example of temperature and pressure fluctuation at 40 °C and 57 bar.

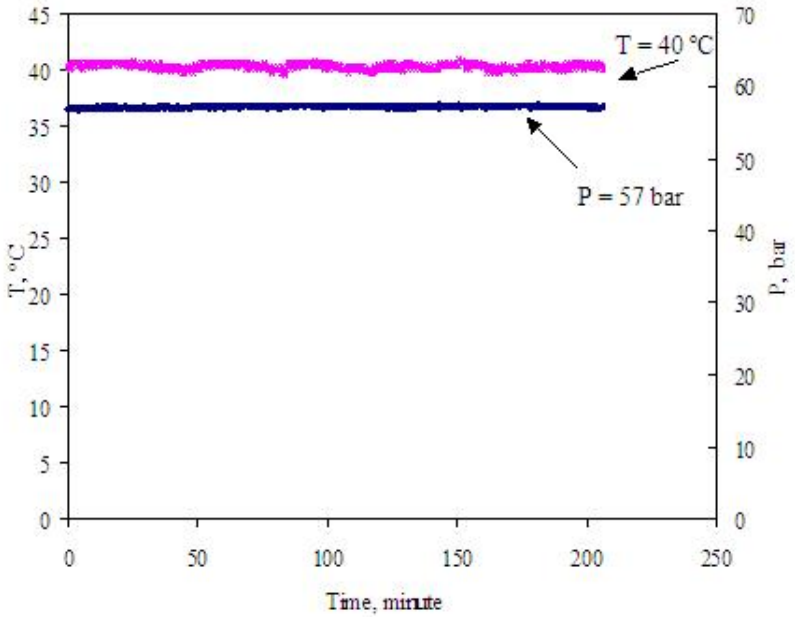

Figure 2.2: Temperature and pressure control at 40 °C and 57 bar

In a typical run, the cell is first evacuated down to a subambient pressure and pre-flushed with designated gas for several times to remove any residue air. Predetermined amount of the liquid mixture is syringed into the cell, followed by addition of a pure gas (CO or H_2) or gas mixtures (H_2/CO_2 or CO/CO_2 with certified compositions by gas suppliers) from the top of the view cell. The system is then brought to the set temperature, stirred, and allowed to equilibrate. A micropump is employed to circulate the vapor through the liquid phase to mix and achieve equilibrium. At each equilibrated pressure, samples are withdrawn from both the vapor and liquid phases and analyzed using an online gas chromatograph. During each sample withdrawal, two sample loops are filled simultaneously to enable parallel analysis, where the non-polar gas components are analyzed by Thermal Conductivity Detector (TCD) and the polar organic components by a Flame Ionization Detector

(FID).

2.3 Gas Chromatograph

2.3.1 Gas Chromatograph

Gas Chromatograph is a widely used analytical instrument. Chromatography is a separation method in which the components of a sample partition between two phases [McNair and Miller, 1998]: a stationary bed with a large surface area, and a gas phase which percolates through the stationary bed. The sample is vaporized and carried by the mobile gas phase (the carrier gas) through the column. Briefly, the various components of the gas phase sample partition (equilibrate) into the stationary phase based on their adsorption equilibrium constants at the given temperature and elute at various times depending on their relative vapor pressures and affinities for the stationary phase.

2.3.2 GC Plumbing

The GC used in this work is a Varian CP-3800 custom-built in the production facility of Varian Inc. It was designed specifically to quantitatively measure the compounds of interest in our phase equilibrium measurements. The GC plumbing is shown in Figure 2.3. The two sampling valves were purchased from Valco Instruments Co. Inc. The 8-port valve V1 is a dual liquid sampling valve with two sampling loops measuring 0.2 μL and 0.5 μL in internal volume. The 0.2 μL sample is injected to the TCD. The 0.5 μL sample is injected through the splitter to the FID. The 10-port valve V2 is a dual gas sampling valve with 200 μL and 250 μL external

sample loops. The maximum pressure of the valves is 172 bar (2500 psi) and the maximum temperature is 150 °C. The liquid sampling valve was not placed in heated zones to prevent the sample from vaporizing before injection. Gases are normally injected at high temperature and low pressure to prevent condensation in the lines. The gas sampling valve was placed in contact with an aluminum heating block. The sample valve temperature was set to 100 °C.

The injector is Varian CP-1177 split/splitless injector. The temperature was set to 225 °C. The column oven temperature was set to start from 35 °C, increase in a rate of 10 °C /min till reaches 95 °C, then increase in a rate of 30 °C /min till 205 °C, stay and hold for 10 minutes. The TCD temperature was 225 °C with the filament temperature being 350 °C. The make up flow rate of TCD was 25 ml/min and the reference flow rate was 40 ml/min. The FID temperature was 300 °C. The make up flow rate of FID was 25 ml/min. The H_2 and Zero Air flow rates were 30 ml/min and 300 ml/min separately.

The capillary column used for measuring liquid phase composition was a Varian CP-Wax 52CB, 50m × 0.25 mm× 0.2 μm. The carrier gas was helium. The packed columns used for measuring gas phase composition were a pre-column (4' × 1/16", 1.5% OV-101 on Chromasorb GHP) from Supelco, and a separation column. The separation column was originally ShinCarbon ST, 100/120 meshed, SS, 1m × 1mm from Restek. Because of the lack of repeatability, it was changed to a Hayesep D 6' × 1/8" SS, 80/100 meshed from Hayes Separation Inc. The repeatability was tested by measuring the CO_2 composition in the gas phase of CO_2/acetone mixture at 40 °C

(Figure 2.4). Repeated GC injections obtained with Shincarbon had a variation greater than 5%. Repeated injections with Hayesep D had a variation of less than 3%.

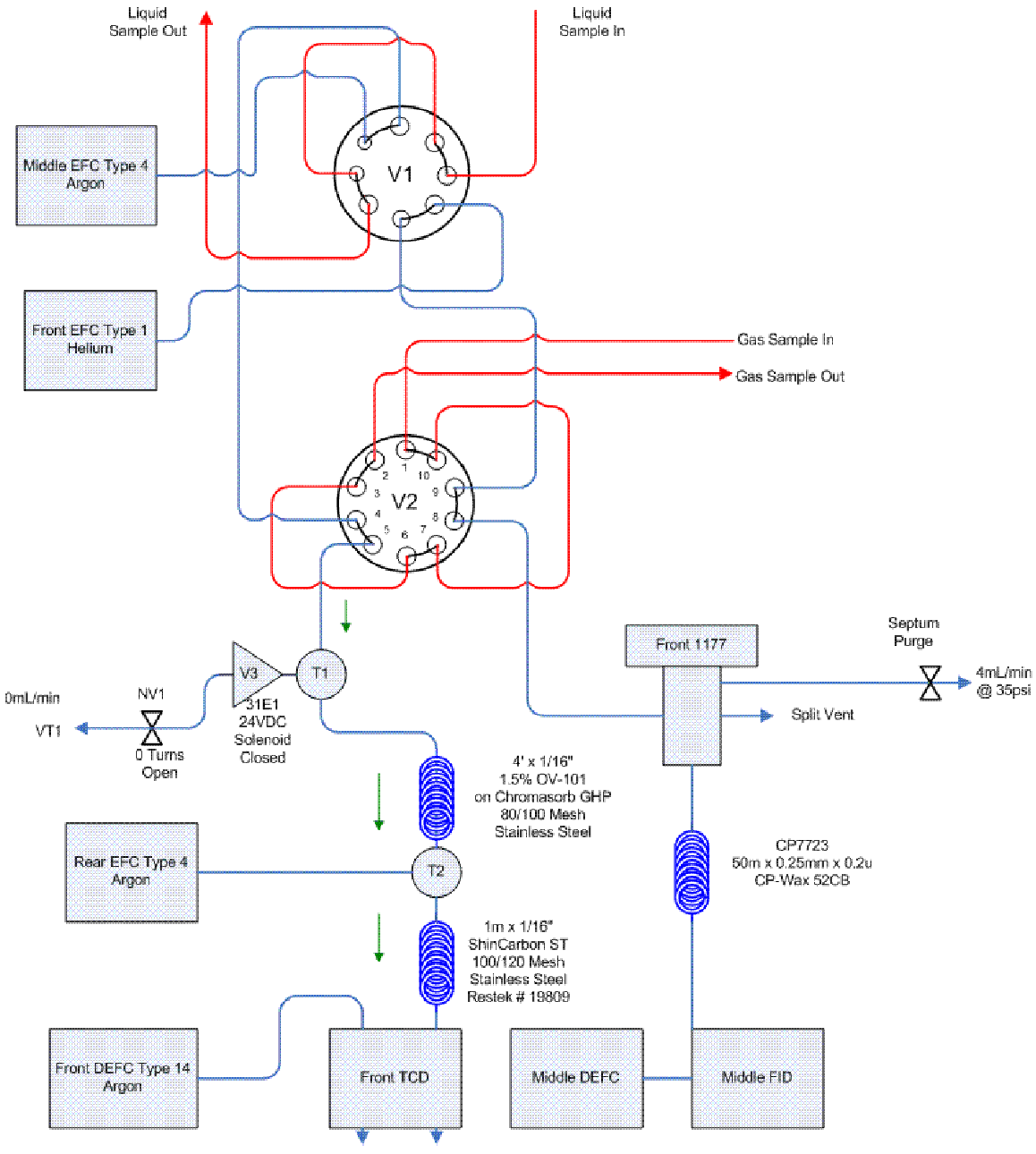

Figure 2.3: Schematic of GC plumbing for sampling liquid and vapor phases

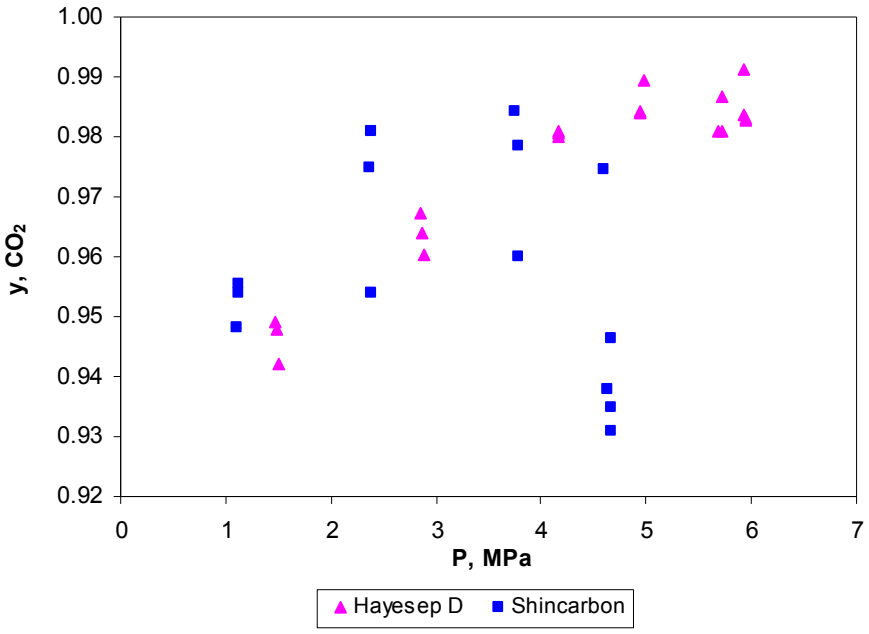

Figure 2.4: CO_2 data repeatability in Hayesep D and Shincarbon packed columns

The carrier gas used for packed column injection is argon in order to enable TCD detection of hydrogen, carbon monoxide and carbon dioxide. Hydrogen is detected with greatly reduced sensitivity when helium carrier gas is used. Besides, the hydrogen peak polarity will reverse from positive to negative as hydrogen concentration increases [Thompson, 1977]. Since the hydrogen concentration is expected to be low in the liquid phase, argon or nitrogen is a better choice than helium as carrier gas. As inferred from Table 2.1, argon is a better choice than N_2 to detect CO by TCD since the relative thermal conductivity difference between CO and argon is more compared to that between N_2 and argon.

Table 2.1: Thermal conductivities of gases

Gas	Relative Thermal Conductivities
Hydrogen	45.9
Helium	36.9
Nitrogen	6.4
Carbon Monoxide	6.2
Argon	4.4
Carbon Dioxide	4.2

2.4 GC Sampling Techniques

The liquid phase is withdrawn from the bottom of the view cell by the micropump, then routed through the liquid sampling valve in the GC and returned back to the cell to the vapor phase at the top. The circulation of the liquid is performed until the system reaches equilibrium as signified by constant temperature, pressure and phase compositions. The liquid phase is sampled by the liquid sampling valve and analyzed by GC.

The vapor phase is sampled by static gas sampling method by withdrawing a small amount of gas from the top of the view cell. A capillary tubing with 0.015" ID × 1/16" OD × 56" L is used as sample transfer line. The pressure drop in the cell upon sampling is usually less than 1 bar. Following each sampling, the pressure is maintained constant by suitably moving the piston.

In order to prevent condensation of the vapor phase sample, the 1/16" sample transfer line connecting the view cell and the GC gas sampling valve is heated to 100 °C, or 40 °C above the temperature of the vapor in the view cell. In order to obtain an

even heating, the 1/16" capillary tubing was jacketed in an 1/8" aluminum tubing. The sample transfer line temperature was measured by a thermocouple, located in a "T" joint roughly 6 inches from the sample inlet to the valve oven of the GC. The thermocouple was connected to a Camile® 3300 data acquisition and control system, which controlled the temperature via a heating cord wrapped in a spiral over the sample line.

Atmospheric balancing [Clevett, 1986] technique was used here to load the sample loop with the gas sample. Atmospheric balancing involved shutting off the sample flow and allowing the pressure in the sample loop to equilibrate with atmospheric pressure at a constant temperature, prior to injection. In this manner, an identical molar amount of the various samples was injected into the GC column. The liquid samples were injected directly under pressure from the LSV.

2.5 Qualitative and Quantitative Analysis

2.5.1 Qualitative Analysis

The superposition of retention time with standards was used to identify each solute. The chromatogram of H_2, CO and CO_2 from a packed column injection is shown in Figure 2.5. The chromatogram of acetone, 1-octene and nonanal from a capillary column injection is shown in Figure 2.6.

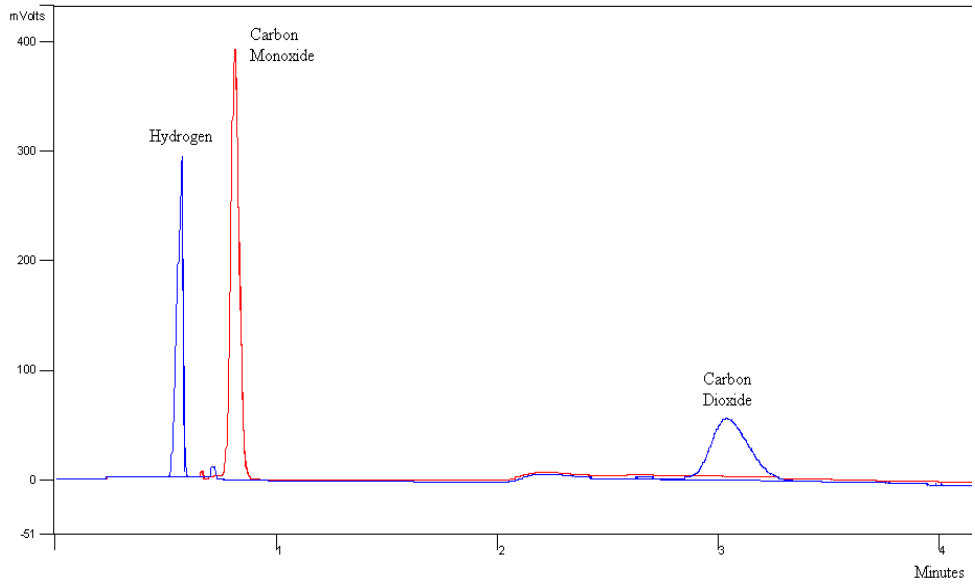

Figure 2.5: GC/TCD chromatogram of H_2, CO and CO_2 (pertinent GC conditions shown in Section 2.3.2)

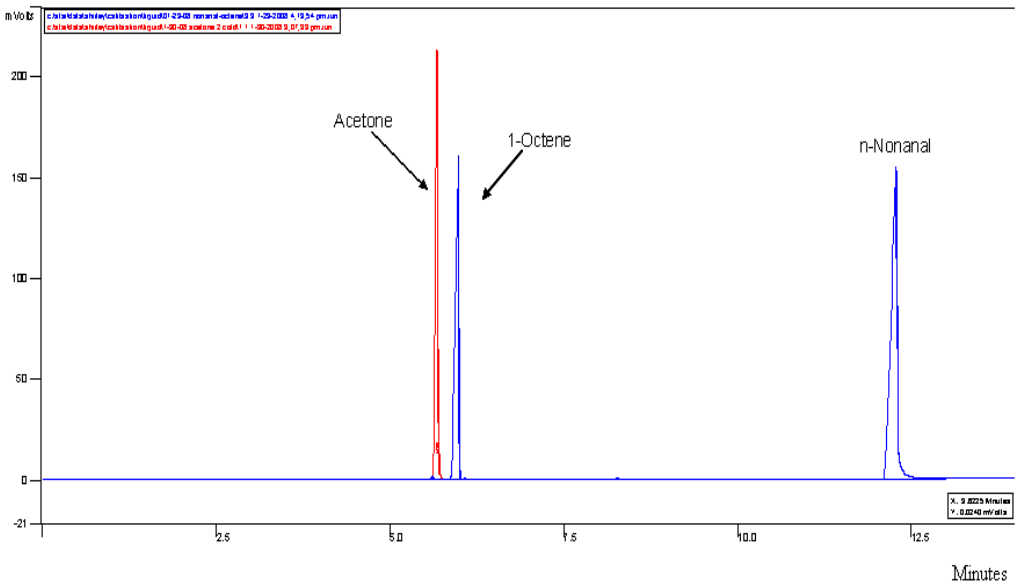

Figure 2.6: GC/FID chromatogram of organics (pertinent GC conditions shown in Section 2.3.2)

2.5.2 Quantitative Analysis

External standardization method was applied to the on-line gas analysis. In this technique, a standard of known composition is chromatographed to generate linear calibration curves for each of the components in the systems being investigated. An identical amount of the sample with unknown composition is then chromatographed. The concentration of a given component is then estimated from the peak areas of that component from the calibration sample and the measured sample.

Calibration curves of gaseous components were generated using the vacuum calibration method by constructing an experimental unit (Figure 2.7) similar to the one described in Thompson (1977). The calibration procedure involves evacuating a gas sampling valve by a vacuum pump to -29 in Hg (-0.97 atm) prior to each injection. The sample loop was then filled with the sample with known composition to a predetermined pressure (less than atmospheric pressure). Because the vapor phase was sampled at atmosphere pressure during the solubility measurement experiments, the concentrations obtained here were normalized to atmosphere pressure (760 mm Hg). In other words:

$$x = \frac{P}{P_{atm}} x' \qquad \text{(Equation 2.1)}$$

where x = normalized concentration (mole%)

P = pressure in the sample loop (mm Hg)

x’ = concentration in the gas standard (mole%)

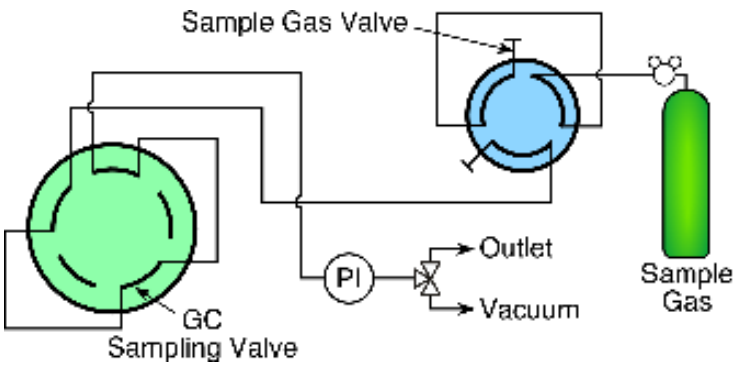

Figure 2.7: Schematic of vacuum calibration method

A range of pressures was chosen to produce concentrations that bracket the feed and expected product concentrations. Three repeat injections were made for each pressure (i.e., concentration). Concentration versus peak area curves was thus generated for each gaseous component.

Calibration curves for the liquid samples were obtained by manual injections using Hamilton microliter syringes (10 µL, 701N, 80300) with a Hamilton Chaney Adapter (700, 14700) to increase reproducibility. A series of liquid samples with known concentrations was first prepared and then manually injected into the GC using microliter syringes. At least three repeat injections were made for each concentration to check for reproducibility. Concentrations versus peak area curves were thus generated. When injecting acetone containing liquids, the samples were first refrigerated till below -10 °C to reduce the loss of acetone by evaporation.

The calibration curves and data sheets are included in the Appendix A. The standard deviation was within 4 % at each data point.

2.6 Error Analysis

2.6.1 Sources of Errors

Experimental measurements are in error or contain uncertainty for a variety of reasons. These can be grouped into three categories: blunders, bias, and random error [Preston, 1986].

Blunders includes such things as incorrectly reading a scale, transposing digits when recording data, using substance A and assuming it is substance B in a process, unintentional omission of known, recognized key steps in a process and not being aware of them and incorrect calculations. The list of blunders can be very large. Unfortunately, we have little hope of eliminating blunders completely. The only sure way to eliminate their effect is to have independent repetition of the measurement. In this work, the experimental data were compared with literature data in order to demonstrate the effect of blunders was small or eliminated.

Bias is sometimes called “systematic error”. It is error caused by consistent factors that cause the same type of error in every observation of a given measurement. In this work, bias was reduced by calibrating all the measuring instruments such as thermocouples, pressure transducers and balance before use, as well as careful handling and control of the experiments.

Random error was reduced by repeated measurements.

A list of instrument precisions is showed in Table 2.2.

Table 2.2: Instrument Precisions

Instrument	Measurement Range	Precision
Electronic Scale	0 ~ 210 g	± 0.1 mg
Micrometer syringe	0 ~10 μL	± 0.01 μL
Vacuum Gauge	-30 mmHg Vac ~ 100 psi	± 0.25%
Thermocouple (RTD)	0 ~ 150 °C	± 0.5 °C
Pressure Transducer	-1 ~ 200 bar	± 0.14 bar

2.6.2 Standard Deviation

Replicates enable the error sum of squares in the analysis of variance. The most widely used measure of uncertainty, dispersion, or "error" is the standard deviation or more properly the "sample standard deviation" [Preston, 1986]. This quantity, called a "statistic" (*s*), is computed from Equation 2.2.

$$s^2 = \frac{\sum_{i=1}^{i=N} (X_i - \overline{X})^2}{N} \qquad \text{(Equation 2.2)}$$

where X_i = computed or measured property

X = arithmetic average of X_i (also called the mean)

N = number of measurements

The term s^2 (i.e. the square of the standard deviation) is so frequently encountered and used in statistical notation that it is given a separate name, i. e. variance. The standard deviation has some unique characteristics that make it well suited for stating the dispersion or uncertainty in a set of measurements. There are two standard

deviations: (1) the sample standard deviation, defined by Equation 2.2, and (2) the "sample estimate of the population standard deviation" defined by Equation 2.3:

$$s_P^2 = \frac{\sum_{i=1}^{i=N} (X_i - \overline{X})^2}{N-1} \qquad \text{(Equation 2.3)}$$

These differ only by N and N-1 in the denominator. One uses Eq. 2.2 when discussing the uncertainties in a given experimental set of measurements, when one is not trying to characterize variability in the "world of all possible such measurements". One uses Equation 2.3 when establishing the uncertainty for the entire (infinite) set of such measurements. Hence, Equation 2.3 was used to measure the dispersions or standard deviations in this.

2.6.3 Error Associated with Calculated Concentrations

The confidence intervals for calibration were chosen as error terms for this research. Linear regression served as a basis for the discussion of calibration intervals. Bonate [1992] discussed error calculations for chromatography in a series of four articles. These articles were used as the reference of the error analysis.

The linear regression model is [Walpole, 2002]:

$$y_i = \hat{y}_i + E_i$$
$$\hat{y}_i = a + bx_i \qquad \text{(Equation 2.4)}$$

where y_i = value of a random variable corresponding to a fixed observation x_i

x_i = independent regressor variable (fixed, not random)

$\hat{y}_i$ = value of y predicted by regression

a = estimate of the intercept of the model regression line (a parameter)

b = estimate of the slope of the model regression line (a parameter)

E_i = model error

The regressor (x) variable is assumed to be non-random in the derivation of variance terms for a and b in eq. 2.4. In other words, x is required to be fixed or measured with negligible error relative to the dependent variable y. When generating the calibration curves for gas chromatography using standard, concentration is the fixed or measured variable and peak area is the dependent variable. Intercept a is assumed to be zero, i.e. when there is no gas concentration, there will be no peak showing up. From Equation 2.4, we get

$$y_i = bx_i + E_i \qquad \text{(Equation 2.5)}$$

To calculate the lower and upper confidence limits for calibration, first, an expression was obtained for the slope estimate of a line through the origin [Neter and Wasserman, 1974]:

$$b = \frac{\sum_{j=1}^{n} x_j y_j}{\sum_{j=1}^{n} x_j^{\,2}} \qquad \text{(Equation 2.6)}$$

where x_j, y_j = data points used to generate the regressed line

n = total number of data points used in the regression

b = regressed slope of the calibration curve

After solving a series of equations, the expression for the lower and upper confidence limit of calculated concentration was obtained [Snavely, 1996]:

$$L1 = \frac{by_i - ts\sqrt{b^2 + \left(\left(y_i^2 - t^2 s^2\right) \Big/ \sum_{j=1}^{n} x_j^2\right)}}{b^2 - \left(t^2 s^2 \Big/ \sum_{j=1}^{n} x_j^2\right)} \qquad \text{(Equation 2.7)}$$

$$L2 = \frac{by_i + ts\sqrt{b^2 + \left(\left(y_i^2 - t^2 s^2\right) \Big/ \sum_{j=1}^{n} x_j^2\right)}}{b^2 - \left(t^2 s^2 \Big/ \sum_{j=1}^{n} x_j^2\right)} \qquad \text{(Equation 2.8)}$$

where t = Student's t-distribution with a 100% probability

L1 = lower confidence limit of calculated concentration

L2 = upper confidence limit of calculated concentration

The slope and residual mean square values obtained from an Excel 2002 regression of the data through the origin are substituted for b and s^2 in eq. 2.7 and 2.8 when calculating L1 and L2. The sum of the x_j^2 terms can be calculated from the data. The t value can be found from t distribution table [Preston, 1986] based on the probability and degree of freedom. The probability was chosen to be 99%, which means that 99% of the time, the true value of y lies between L1 and L2 [Mickley, 1957]. The percent error of L1 and L2 (e.g. the difference of y_j and L1, divided by y_j) were also calculated. All of the error calculation results are shown with the calibration data table in Appendix A.

CHAPTER 3 VAPOR LIQUID EQUILIBRIUM DATA AND MODELING

The experimental VLE data for the following systems are presented in this chapter: CO_2/acetone, CO/1-octene, CO_2/1-octene, CO/nonanal, CO_2/nonanal, H_2/1-octene, H_2/nonanal binary systems and CO/CO_2/acetone, CO/CO_2/1-octene, CO/CO_2/nonanal, H_2/CO_2/1-octene ternary systems. The binary and ternary systems are also modeled using empirical equations of state in order to develop predictive models.

3.1 Materials

1-Octene (99+ % purity) was obtained from Acros Organics, nonanal (lot purity ⩾ 99%) was obtained from Sigma-Aldrich Inc., and acetone (HPLC Grade 99.9+ %) was acquired from Sigma-Aldrich Inc. All organic compounds were used as received. Carbon dioxide (industrial grade, >99.5%), carbon monoxide (research grade, 99%), hydrogen (ultrahigh purity, 99.99%), and custom gas mixtures were purchased from Airgas Inc. The CO_2/CO gas mixture was 50.00% CO_2 (molar) and the balance was CO; the CO_2/H_2 gas mixture was 50.86% CO_2 (molar) and the balance H_2.

3.2 Benchmarking

In order to establish the reliability of the experimental unit and procedures, a set of benchmarking experiments was performed aimed at reproducing published phase behavior data.

3.2.1 Binary Phase Equilibrium

The vapor-liquid equilibrium (VLE) of CO_2/acetone binary system was measured

at 40 ^{o}C and pressures between 1 and 8 MPa. The VLE data was shown in Tables 3.1 and 3.2, and plotted in Figure 3.1. The mole fractions of CO_2 and acetone in each phase added up to 1. For clarity, only the CO_2 mole fractions were shown in the tables, with the balance being acetone. Mole fractions for the liquid and vapor components were determined analytically by gas chromatograph. Two repeat runs were performed under identical condition. The measurement errors are within the size of the data points. The phase equilibrium data of CO_2 in neat acetone reported by Day [1996] and Katayama [1975] at 40 ^{o}C are also included in Figure 3.1. The experimental data obtained in this work match well with Day and Katayama's data. The VLE data of Day and Katayama under the same pressure of this work was calculated by fitting the VLE curves and included in Table 3.1 and 3.2.

Table 3.1: VLE data of CO_2/acetone at 40 ^{o}C (run 1)

P, MPa	This Work		Day	Katayama	This Work		Day	Katayama
	y (CO_2)	s	y (CO_2)	y (CO_2)	x (CO_2)	s	x (CO_2)	x (CO_2)
2.22	0.953	0.003	0.960	0.963	0.339	0.003	0.330	0.318
3.99	0.969	0.003	0.979	0.980	0.536	0.008	0.542	0.533
5.01	0.976	0.003	0.983	0.984	0.651	0.005	0.664	0.658
5.92	0.985	0.005	0.983	0.986	0.787	0.008	0.774	0.768

s: standard deviation

Table 3.2: VLE data of CO_2/acetone at 40 ^oC (run 2)

P, MPa	This Work		Day	Katayama	This Work		Day	Katayama
	y (CO_2)	s	y (CO_2)	y (CO_2)	x (CO_2)	s	x (CO_2)	x (CO_2)
1.49	0.946	0.004	0.947	0.953	0.251	0.001	0.242	0.229
2.87	0.964	0.003	0.969	0.970	0.402	0.003	0.408	0.397
4.16	0.980	0.001	0.980	0.981	0.550	0.004	0.562	0.554
4.95	0.986	0.003	0.983	0.984	0.638	0.005	0.657	0.650
5.72	0.983	0.003	0.983	0.986	0.754	0.001	0.750	0.744

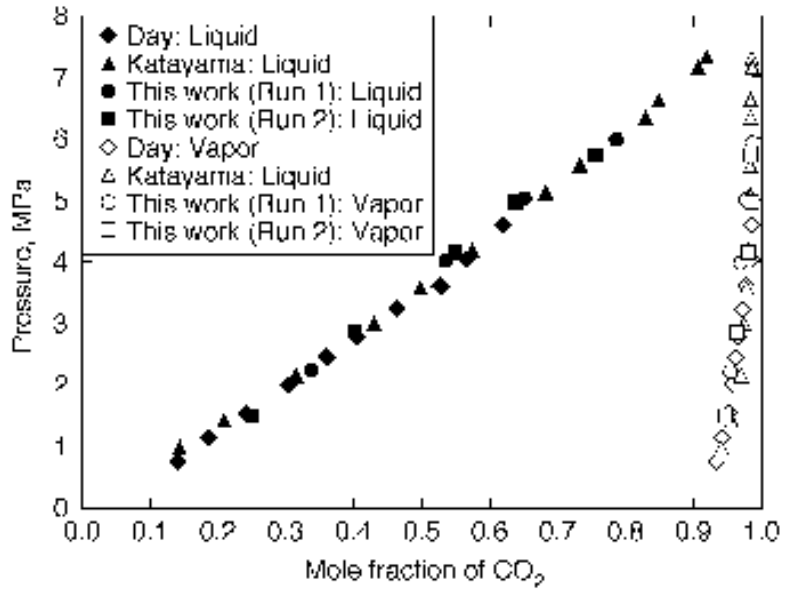

Figure 3.1: VLE of CO_2/acetone at 40 ^oC

The vapor-liquid equilibrium of CO and 1-octene mixture at 60 ^oC and pressures between 1 and 9 MPa were measured and compared with the data of Jin [2006] (Figure 3.2). The errors are within the size of the plotted data points. The data from this work match well with Jin's data. The VLE data are shown in Table 3.3. The mole

fractions of CO and octene in each phase added up to 1. For clarity, only the CO mole fractions were shown in the tables, with the balance being acetone. The VLE data of Jin under the same pressure of this work was calculated by fitting the VLE curves and included in Table 3.3.

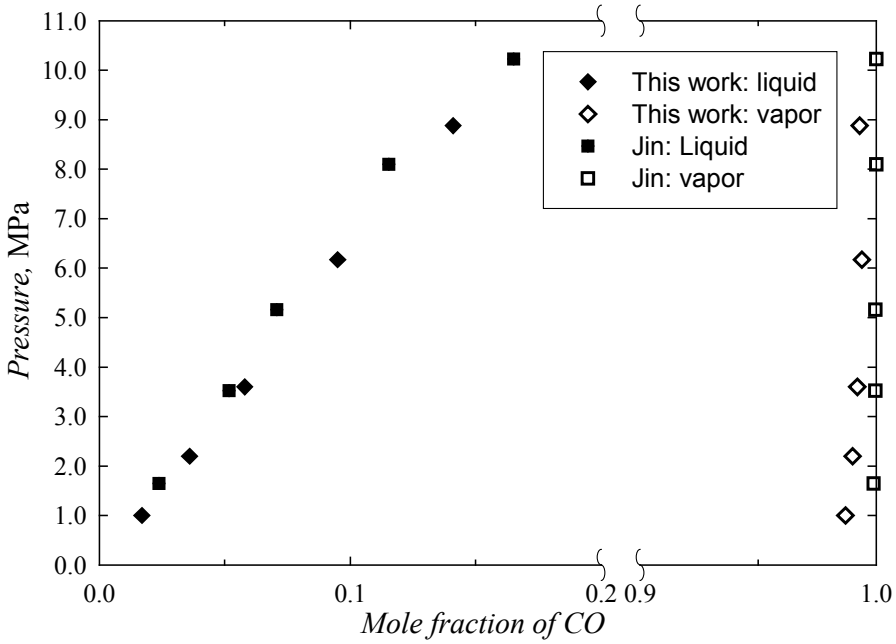

Figure 3.2: VLE of CO/1-octene at 60 ^{o}C

Table 3.3: VLE data of CO/1-octene at 60 ^{o}C

P, MPa	This Work		Jin	This Work		Jin
	y (CO)	s	y (CO_2)	x (CO)	s	x (CO)
1.00	0.987	0.001	0.999	0.017	0.001	0.009
2.20	0.99	0.002	0.999	0.036	0.002	0.028
3.60	0.992	0.001	0.999	0.058	0.003	0.050
6.17	0.994	0.002	1.000	0.095	0.001	0.092
8.88	0.993	0.006	1.000	0.141	0.003	0.135

3.2.2 Ternary Phase Equilibrium

The phase equilibrium of ternary system CO/CO_2/acetone at 40 ^oC and 90 bar was investigated with different gas compositions (Table 3.4). Every entry in Table 3.4 represents a tie line. Several different tie lines were obtained at a given pressure. The mole fractions of CO, CO_2 and acetone in each phase added up to 1. For clarity, only the CO_2 and CO mole fractions were shown in the table, with the balance being acetone.

The results were compared with the data reported by Lopez-Castillo et al. [2006] as shown in Figure 3.3. The experimental data from this work display an identical trend as the literature data and the ends of the tie lines from the two sets of data appear to form a smooth two-phase envelope.

Table 3.4: VLE data of CO/CO2/acetone at 40 ^oC and 90 bar

	y, CO	s (CO)	y, CO_2	s (CO_2)
Vapor Phase	0.656	0.0011	0.314	0.0027
	0.450	0.0039	0.510	0.0026
	0.173	0.0015	0.801	0.005
	0.252	0.0044	0.725	0.0066
	x, CO	s (CO)	x, CO_2	s (CO_2)
Liquid Phase	0.065	0.0008	0.318	0.0022
	0.061	0.001	0.515	0.0043
	0.054	0.0007	0.822	0.0013
	0.054	0.0002	0.774	0.0001

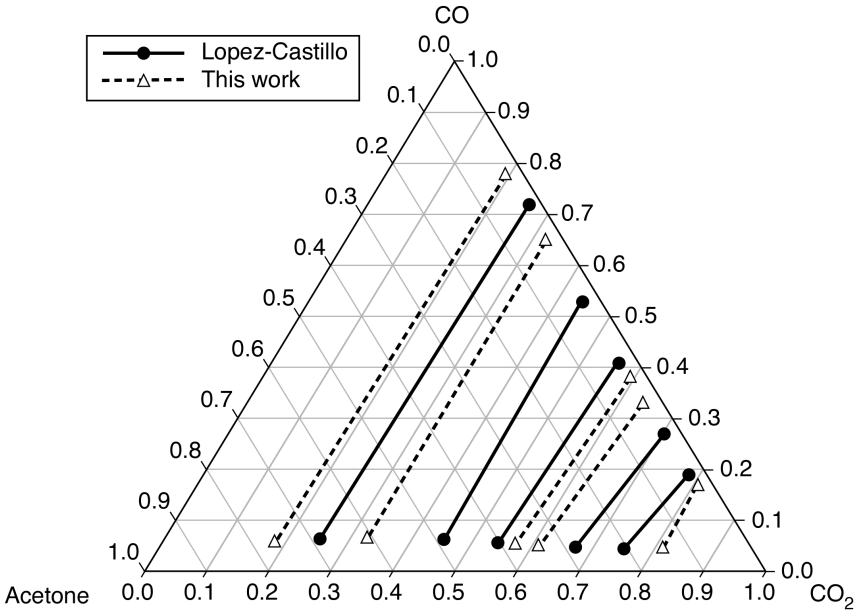

Figure 3.3: VLE of CO/CO_2/acetone at 40 ^oC and 90 bar

3.3 Phase Equilibrium of CO in Neat and CO_2-Expanded Solvents

3.3.1 VLE of CO/1-Octene and CO_2/1-Octene Binary Systems

The vapor-liquid equilibrium of CO and 1-octene mixture was measured at 40 ^oC, 60 ^oC, 80 ^oC and at pressures between 1 and 9 MPa at each temperature. The data are plotted in Figure 3.4. The errors are within the size range of the plotted data points. In general, the solubility of CO increases with an increase in total pressure. In contrast, temperature has a weak effect on CO solubility in the liquid phase.

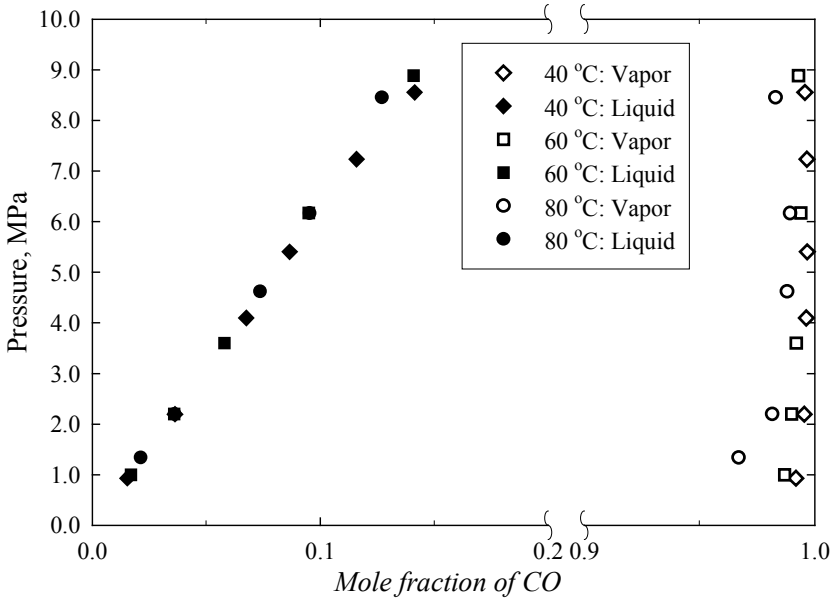

Figure 3.4: VLE of CO/1-octene at 40 °C, 60 °C and 80 °C

The VLE data of CO/1-octene at 40 °C, 60 °C and 80 °C are shown in Tables 3.5, 3.2 and 3.6 respectively.

Table 3.5: VLE data of CO/1-octene at 40 °C

P, Mpa	x, CO	x, 1-Octene	s	y, CO	y, 1-Octene	s
0.93	0.015	0.985	0.001	0.992	0.008	0.001
2.20	0.036	0.964	0.001	0.995	0.005	0.001
4.10	0.068	0.932	0.001	0.996	0.004	0.001
5.40	0.087	0.913	0.003	0.997	0.003	0.001
7.23	0.116	0.884	0.005	0.997	0.003	0.001
8.55	0.141	0.859	0.002	0.996	0.004	0.001

Table 3.6: VLE data of CO/1-octene at 80 ^{o}C

P, Mpa	x, CO	x, 1-Octene	s	y, CO	y, 1-Octene	s
1.34	0.021	0.979	0.001	0.967	0.033	0.003
2.20	0.036	0.964	0.002	0.982	0.018	0.000
4.62	0.074	0.926	0.003	0.988	0.012	0.001
6.16	0.095	0.905	0.001	0.989	0.011	0.001
8.45	0.127	0.873	0.004	0.983	0.017	0.009

Henry's law constants were calculated using Equation 3.1:

$$K_H = P / x \qquad \text{(Equation 3.1)}$$

The results were compared with the literature data of Purwanto et al [1996] and Jauredui-Haza et al [2004] (Table 3.7).

Table 3.7: Henry's Law constants for CO in 1-octene at various temperatures

T, ^{o}C	10^{-5} *K_H, Mpa	Reference
40	62.1	This work
50	63	Purwanto et al.
60	63.3	This work
80	64.9	This work
80	74.9±1.1	Jauredui-Haza et al.
90	72.8±1.5	Jauredui-Haza et al.
100	75.5±1.7	Jauredui-Haza et al.

The Henry's law constants obtained in the present study are in good agreement with the literature data of Purwanto et al [1996]. However, the Henry's law constant at 80 ^{o}C is approximately 15% less than the values reported by Jauredui-Haza et al

[2004].

The vapor-liquid equilibrium data for CO_2 and 1-octene binary mixtures at 40 ^oC, 60 ^oC and 80 ^oC at pressures between 1 and 9 MPa are plotted in Figure 3.5. The errors are within the size ranges of the data points. As expected, the CO_2 solubility in 1-octene increases with an isothermal increase in pressure while an increase of temperature reduces the CO_2 solubility in 1-octene.

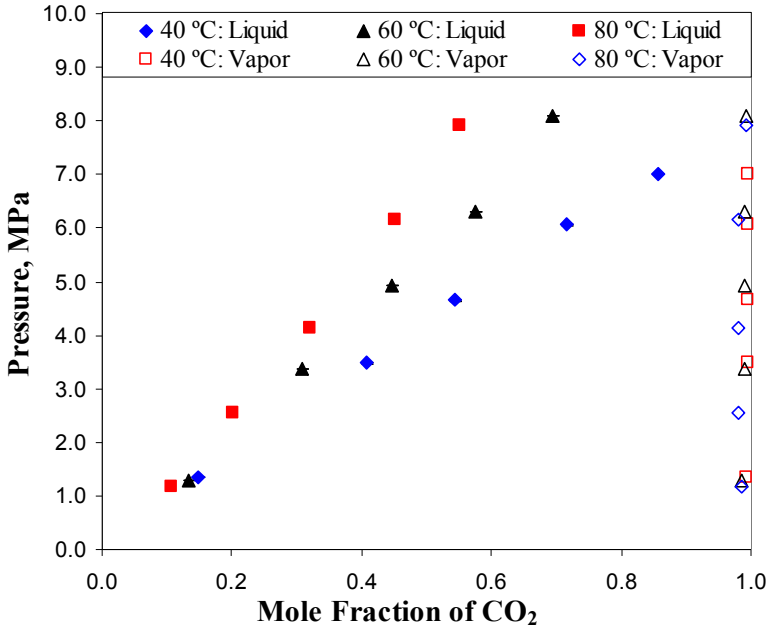

Figure 3.5: VLE of CO_2/1-octene binary at 40 ^oC, 60 ^oC and 80 ^oC

The VLE data of CO_2/1-octene binary mixtures at 40 ^oC, 60 ^oC and 80 ^oC are shown in Tables 3.8, 3.9 and 3.10 respectively.

Table 3.8: VLE data of CO_2/1-octene at 40 ^oC

P, Mpa	x, CO_2	x, 1-octene	s	y, CO_2	y, 1-octene	s
1.35	0.147	0.853	0.0056	0.993	0.007	0.0006
3.48	0.408	0.592	0.0079	0.995	0.005	0.0001
4.65	0.544	0.456	0.0021	0.996	0.004	0.0000
6.06	0.717	0.283	0.0050	0.994	0.006	0.0007
7.01	0.858	0.142	0.0028	0.995	0.005	0.0002

Table 3.9: VLE data of CO_2/1-octene at 60 ^oC

P, Mpa	x, CO_2	x, 1-octene	s	y, CO_2	y, 1-octene	s
1.28	0.134	0.866	0.005	0.985	0.015	0.0003
3.37	0.307	0.693	0.007	0.991	0.009	0.0002
4.94	0.446	0.554	0.004	0.991	0.009	0.0006
6.31	0.576	0.424	0.006	0.990	0.010	0.0001
8.09	0.694	0.306	0.002	0.994	0.006	0.0014

Table 3.10: VLE data of CO_2/1-octene at 80 ^oC

P, Mpa	x, CO_2	x, 1-octene	s	y, CO_2	y, 1-octene	s
1.17	0.107	0.893	0.005	0.985	0.015	0.0003
2.55	0.201	0.799	0.007	0.980	0.020	0.0002
4.13	0.320	0.680	0.004	0.980	0.020	0.0006
6.17	0.452	0.548	0.006	0.980	0.020	0.0001
7.91	0.551	0.449	0.002	0.994	0.006	0.0014

3.3.2 VLE of CO/CO_2/1-Octene Ternary Systems

The VLE phase equilibrium data of the CO/CO_2/1-octene ternary system at 40 ^oC, 60 ^oC and 80 ^oC at 8 MPa are provided in Tables 3.11, 3.12 and 3.13 respectively.

Table 3.11: VLE data of CO/CO_2/1-octene at 40 ^oC and 8 MPa

	y, CO	s, CO	y, CO_2	s, CO_2	y, CO (HYSYS)	y, CO_2 (HYSYS)
Vapor Phase	0.273	0.001	0.723	0.001	0.273	0.724
	0.382	0.003	0.614	0.003	0.382	0.614
	0.491	0.004	0.505	0.004	0.492	0.505
	0.556	0.006	0.440	0.006	0.556	0.440
	x, CO	s, CO	x, CO_2	s, CO_2	x, CO (HYSYS)	x, CO_2 (HYSYS)
Liquid Phase	0.042	0.001	0.571	0.002	0.045	0.568
	0.056	0.002	0.485	0.000	0.058	0.472
	0.068	0.001	0.399	0.002	0.070	0.384
	0.074	0.001	0.347	0.002	0.077	0.334

Table 3.12: VLE data of CO/CO_2/1-octene at 60 ^oC and 8 MPa

	y, CO	s, CO	y, CO_2	s, CO_2	y, CO (HYSYS)	y, CO_2 (HYSYS)
Vapor Phase	0.261	0.001	0.732	0.001	0.261	0.733
	0.348	0.003	0.645	0.003	0.348	0.646
	0.469	0.004	0.524	0.004	0.469	0.525
	0.573	0.006	0.420	0.006	0.573	0.421
	x, CO	s, CO	x, CO_2	s, CO_2	x, CO (HYSYS)	x, CO_2 (HYSYS)
Liquid Phase	0.036	0.001	0.458	0.002	0.037	0.447
	0.047	0.002	0.403	0.000	0.049	0.392
	0.062	0.001	0.328	0.002	0.065	0.315
	0.074	0.001	0.262	0.002	0.077	0.251

Each row in these tables represents the ends of a tie line. Several different tie lines were obtained at a given pressure. The mole fractions of CO, CO_2 and 1-octene in each phase add up to 1. For clarity, only the CO_2 and CO mole fractions are shown in the table, with the balance being 1-octene. The modeled VLE data are compared with the experimental data in Tables 3.11-3.13.

Table 3.13: VLE data of CO/CO_2/1-octene at 80 ^oC and 8 MPa

	y, CO	s, CO	y, CO_2	s, CO_2	y, CO (HYSYS)	y, CO_2 (HYSYS)
Vapor Phase	0.267	0.0009	0.721	0.001	0.267	0.719
	0.360	0.0004	0.628	0.001	0.360	0.627
	0.451	0.0002	0.537	0.001	0.451	0.536
	0.554	0.0035	0.434	0.004	0.554	0.435
	x, CO	s, CO	x, CO_2	s, CO_2	x, CO (HYSYS)	x, CO_2 (HYSYS)
Liquid Phase	0.038	0.001	0.396	0.003	0.041	0.388
	0.050	0.001	0.345	0.002	0.053	0.335
	0.060	0.001	0.295	0.002	0.064	0.286
	0.073	0.001	0.239	0.003	0.076	0.232

The VLE data for the ternary systems were simulated at the experimental conditions by using Aspen HYSYS software with the Peng-Robinson equation of state (PR EoS) , van der Waals mixing rules and binary interaction parameters. The experimental temperature, pressure are specified for a single feed. The experimental vapor phase composition was used as the feed composition in the flash calculation. When no results were obtained in the two-phase region, then slightly richer organic

compositions were used lying approximately in the same experimental tie line. A flash calculation is carried out by HYSYS under the specified conditions with chosen thermo model (PR EoS). The objective function used for fitting is given by Equation 3.2 with a convergence criterion of less than 10^{-4} for both liquid and vapor phase compositions. All of the critical properties T_c, P_c, ω are from HYSYS internal library.

Table 3.14: Binary interaction parameters used in the PR EoS

Compounds		T (°C)	k_{ij}	Comments
CO_2	CO	40	0.21	used as reported [Lopez-Castillo et al., 2006]
		60	0.27	extrapolated from k_{ij} values fit to literature data [Christiansen et al., 1974; Lopez-Castillo et al., 2006]
		80	0.31	extrapolated from k_{ij} values fit to literature data [Christiansen et al., 1974; Lopez-Castillo et al., 2006]
CO_2	1-octene	40	0.08	fit to experimental data of this work
		60	0.09	fit to experimental data of this work
		80	0.10	fit to experimental data of this work
CO	1-octene	40	0.02	fit to experimental data of this work
		60	0.02	fit to experimental data of this work
		80	0.02	fit to experimental data of this work

The binary interaction parameters used were obtained from literature data if available. For some systems, when the literature data of binary interaction parameter are not available, the HYSYS® simulator was used to generate the binary interaction parameters by fitting the experimental VLE data for the binary system. When data

were not available at the temperature of interest, k_{ij} values were interpolated or extrapolated from the temperatures available. In Table 3.14, the binary interaction parameters used in the simulation are reported.

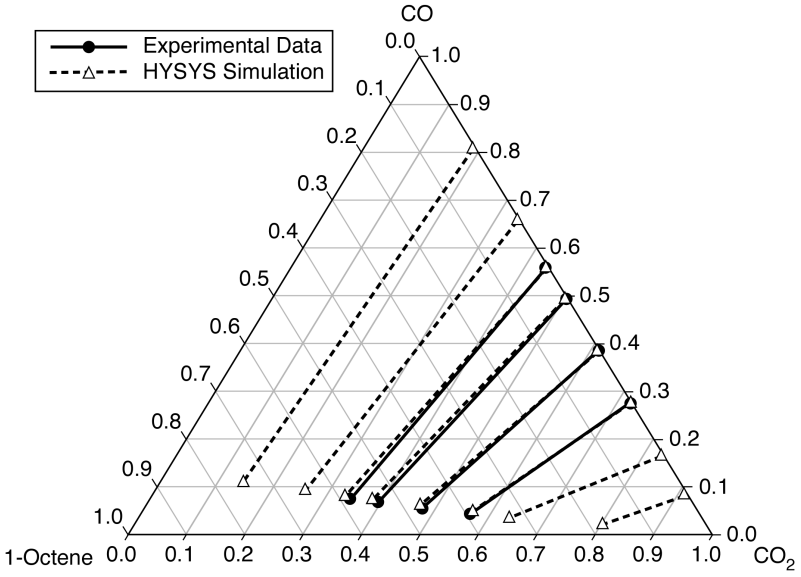

Figure 3.6: VLE of CO/CO_2/1-octene at 40 ^oC and 8 MPa

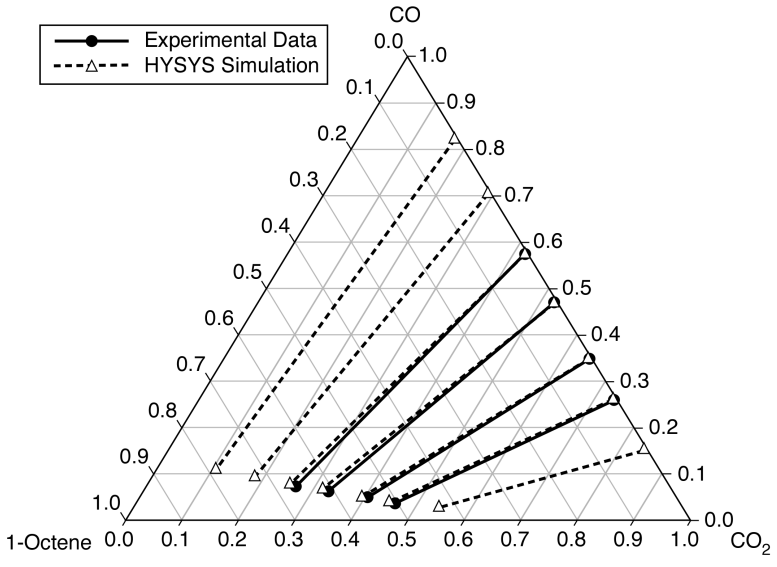

Figure 3.7: VLE of CO/CO_2/1-octene at 60 ^oC and 8 MPa

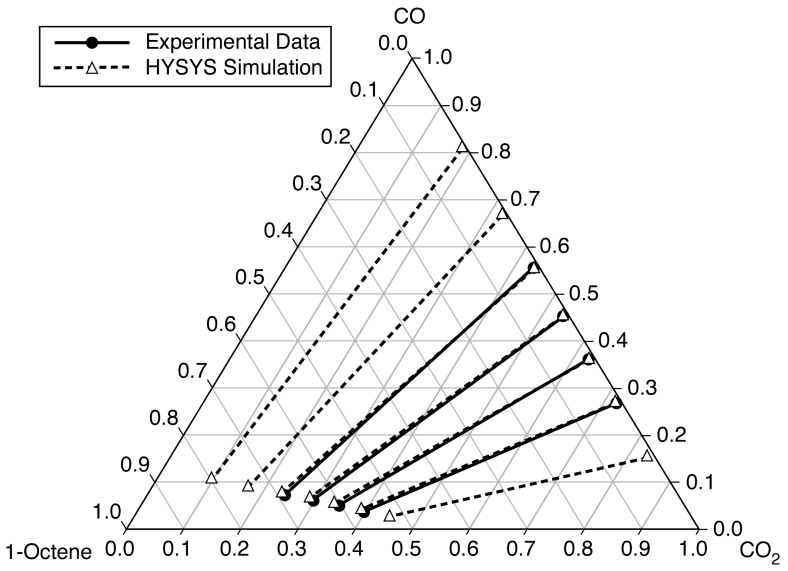

Figure 3.8: VLE of CO/CO_2/1-octene at 80 ^oC and 8 MPa

The experimental and simulated VLE data for the CO/CO_2/1-octene ternary system at 40 ^oC, 60 ^oC and 80 ^oC and 8 MPa are shown in Figures 3.6, 3.7 and 3.8 respectively. The experimental and calculated values were compared using the percent absolute average deviations (%AARD) defined as follows:

$$\%AARD = \frac{100}{ND}\sum_{1}^{ND}\frac{\left|x_{\exp} - x_{cal}\right|}{x_{\exp}} \qquad \text{(Equation 3.2)}$$

Where *ND* stands for the number of data, x_{exp} and x_{cal} stand for the experimental and calculated mole fractions separately.

Since the vapor phase compositions were used as feed composition. The modeling results of the vapor phase compositions fit extremely well with the experimental results. The results for the liquid phase compositions were reported in Table 3.15. In general, the results matched the experimental data reasonably well. The good fit between the experimental data and simulated results is attributed to the fact that the

CXL phase (compositions close to the 1-octene/CO axis in Figures 3.6-3.8) is lean in CO and the gas phase (compositions closer to the CO/CO_2 axis) are lean in 1-octene, and these two phases may thus be approximated as pseudo-binary systems.

Table 3.15: %AARD for HYSYS Modeling using Peng-Robinson EoS

CO(1)/CO_2(2)/1-Octene(3)	%AARD		
	x_1	x_2	x_3
40 ^oC	3.03	2.68	1.31
60 ^oC	3.40	2.17	1.35
80 ^oC	5.08	2.20	0.69

In order to better understand the effect of CO_2 on the CO solubility, the CO solubilities in CO_2-expanded solvents are compared with the CO solubility in pure solvent (i.e., without CO_2) at the same temperature and identical CO fugacity in the gas phase. The CO fugacity coefficients at various total pressures were estimated using the Peng-Robinson equation of state. At the experimental conditions, the CO fugacity coefficients were found to be close to unity. An Enhancement Factor (EF) is defined as follows

$$EF = \frac{x_{gas}^{CXL}}{x_{gas}^{neat\ solvent}} \qquad \text{(Equation 3.3)}$$

Where x^{CXL} and $x^{neat\ solvent}$ represent the mole fractions of the permanent gas component in the CXL and neat solvent, respectively. The EF results are shown in Tables 3.16, 3.17 and 3.18.

Table 3.16: Enhancement of CO solubility in CXL (40 ^{o}C, total pressure 8 MPa)

f_{CO}, MPa	x, CO_2 (CXL)	x, CO (CXL)	x, CO (Pure)	EF
2.16	0.571	0.042	0.035	1.20
3.02	0.485	0.056	0.050	1.13
3.88	0.399	0.068	0.064	1.06
4.40	0.347	0.074	0.072	1.02

Table 3.17: Enhancement of CO solubility in CXL (60 ^{o}C, total pressure 8 MPa)

f_{CO}, MPa	x, CO_2 (CXL)	x, CO (CXL)	x, CO (Pure)	EF
2.04	0.458	0.036	0.034	1.08
2.72	0.403	0.047	0.044	1.06
3.67	0.328	0.062	0.060	1.03
4.48	0.262	0.074	0.073	1.02

Table 3.18: Enhancement of CO solubility in CXL (80 ^{o}C, total pressure 8 MPa)

f_{CO}, MPa	x, CO_2 (CXL)	x, CO (CXL)	x, CO (Pure)	EF
2.13	0.396	0.038	0.035	1.09
2.87	0.345	0.050	0.046	1.08
3.60	0.295	0.060	0.057	1.06
4.42	0.239	0.073	0.069	1.02

From Table 3.16-3.18, it may be seen that EF values greater than unity are obtained at all the conditions studied. At constant total pressure, the EF values increase with increasing CO_2 mole fraction in the liquid phase. This increase is attributed to the increase in free volume in the CO_2-expanded liquid phase that favors CO solubility.

3.3.3 VLE of CO/Nonanal and CO_2/Nonanal Binary Systems

Figure 3.9 shows the vapor-liquid equilibrium data for the CO/nonanal system at 40 ^{o}C and 60 ^{o}C and pressures between 1 and 8 MPa. The errors are within the size range of the plotted data points. As expected, the CO solubility increases with total pressure while temperature had a relatively weak affect on the CO solubility.

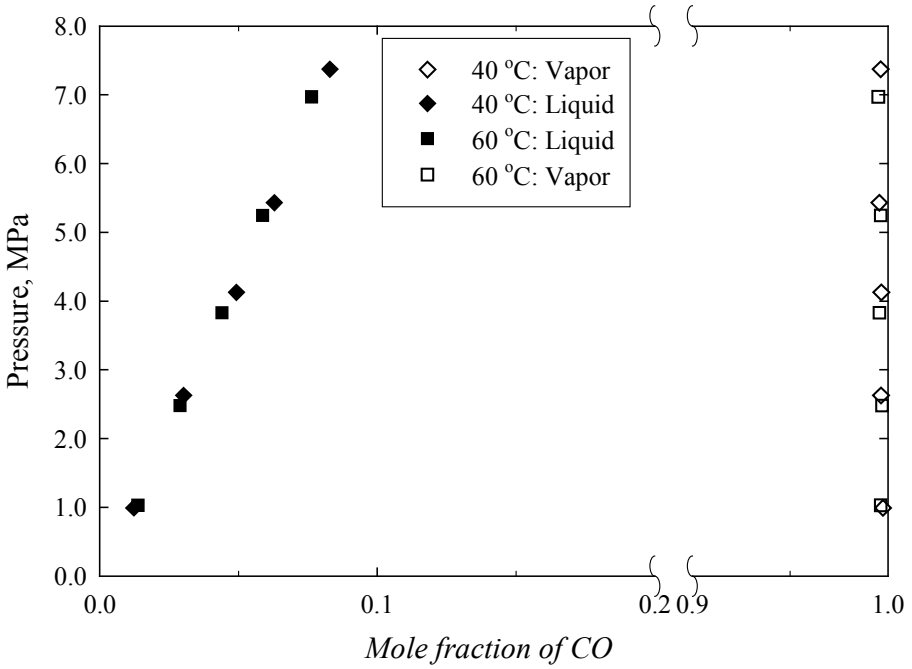

Figure 3.9: VLE of CO/nonanal at 40 ^{o}C and 60 ^{o}C

The VLE data of CO/nonanal at 40 ^{o}C and 60 ^{o}C are summarized in Tables 3.19 and 3.20, respectively.

Table 3.21 shows that the Henry's law constants for CO solubility in nonanal obtained in this work are in good agreement with values reported in the literature.

Table 3.19: VLE data of CO/nonanal at 40 ^{o}C

P, MPa	x, CO	x, Nonanal	s	y, CO	y, Nonanal	s
0.99	0.012	0.988	0.003	0.998	0.002	0.002
2.63	0.030	0.970	0.003	0.996	0.004	0.001
4.13	0.049	0.951	0.005	0.997	0.003	0.002
5.43	0.063	0.937	0.001	0.996	0.004	0.001
7.37	0.083	0.917	0.003	0.996	0.004	0.001

Table 3.20: VLE data of CO/nonanal at 60 ^{o}C

P, MPa	x, CO	x, Nonanal	s	y, CO	y, Nonanal	s
1.03	0.014	0.986	0.001	0.996	0.004	0.000
2.48	0.029	0.971	0.002	0.997	0.003	0.002
3.83	0.044	0.956	0.000	0.996	0.004	0.000
5.25	0.059	0.941	0.001	0.996	0.004	0.001
6.97	0.076	0.924	0.004	0.995	0.005	0.001

Table 3.21: Henry's Law constants for CO in nonanal at various temperatures

T, K	10^{-5} *K_H, MPa	Reference
313	89.3	This work
333	94.3	
353	102.3	Jauredui-Haza et al. [2004]
363	99.3	
373	99.3	

The vapor-liquid equilibrium data for CO_2 and nonanal mixtures at 40 and 60 ^{o}C at pressures between 1 and 8 MPa are shown in Figure 3.10. The experimental error is within the size range of the data points. As expected, the CO_2 solubility in nonanal

increases with total increase and decreases at the higher temperature.

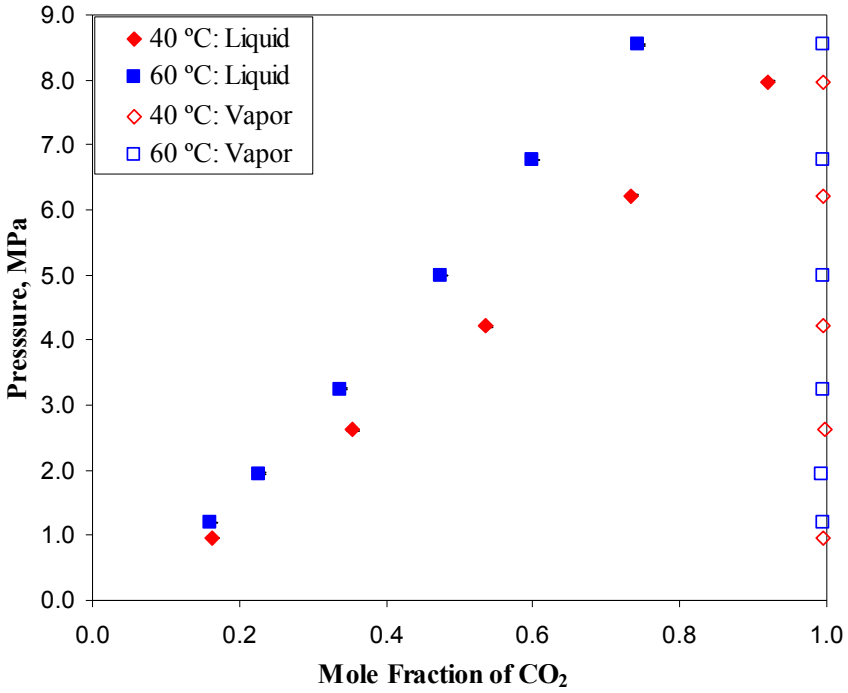

Figure 3.10: VLE of CO_2/nonanal at 40 °C and 60 °C

The VLE data for CO_2/nonanal mixtures at 40 °C and 60 °C are shown in Tables 3.22 and 3.23 respectively.

Table 3.22: VLE data of CO_2/nonanal mixtures at 40 °C

P, MPa	x, CO_2	x, Nonanal	s	y, CO_2	y, Nonanal	s
0.95	0.163	0.837	0.006	0.995	0.005	0.002
2.62	0.354	0.646	0.003	0.997	0.003	0.003
4.21	0.535	0.465	0.003	0.996	0.004	0.002
6.22	0.735	0.265	0.003	0.994	0.006	0.001
7.98	0.920	0.080	0.002	0.995	0.005	0.002

Table 3.23: VLE data of CO_2/nonanal mixtures at 60 ^oC

P, MPa	x, CO_2	x, Nonanal	s	y, CO_2	y, Nonanal	s
1.20	0.161	0.839	0.001	0.995	0.005	0.001
1.95	0.226	0.774	0.002	0.994	0.006	0.002
3.25	0.337	0.663	0.007	0.994	0.006	0.001
5.00	0.475	0.525	0.002	0.996	0.004	0.003
6.77	0.598	0.402	0.007	0.995	0.005	0.001
8.54	0.743	0.257	0.006	0.995	0.005	0.002

3.3.4 VLE of CO/CO_2/Nonanal Ternary Systems

Table 3.24: VLE data for CO/CO_2/nonanal mixtures at 40 ^oC and 8 MPa

	y, CO	s, CO	y, CO_2	s, CO_2	y, CO (HYSYS)	y, CO_2 (HYSYS)
Vapor Phase	0.529	0.002	0.464	0.001	0.535	0.465
	0.319	0.007	0.675	0.005	0.320	0.679
	0.206	0.003	0.791	0.003	0.208	0.792
	0.135	0.006	0.861	0.005	0.137	0.863
	0.396	0.002	0.589	0.002	0.404	0.596
	x, CO	s, CO	x, CO_2	s, CO_2	x, CO (HYSYS)	x, CO_2 (HYSYS)
Liquid Phase	0.054	0.003	0.374	0.003	0.053	0.390
	0.037	0.002	0.613	0.002	0.036	0.559
	0.027	0.001	0.684	0.002	0.026	0.659
	0.021	0.002	0.762	0.004	0.019	0.728
	0.043	0.004	0.517	0.008	0.042	0.494

The VLE data for CO/CO_2/nonanal ternary mixtures at 40 and 60 ^oC at 8 MPa are shown in Tables 3.24 and 3.25. The data in each row of the tables represent a tie line

in a ternary diagram. Several different tie lines were obtained at a given pressure. The mole fractions of CO, CO_2 and nonanal in each phase add up to 1. For clarity, only the CO_2 and CO mole fractions are shown in the tables, with the balance being nonanal. The standard deviations (s) associated with the measurements and the VLE data simulated using HYSYS® are also included in Tables 3.24 and 3.25.

Table 3.25: VLE data of CO/CO_2/nonanal at 60 ^oC and 8 MPa

	y, CO	s, CO	y, CO_2	s, CO_2	y, CO (HYSYS)	y, CO_2 (HYSYS)
Vapor Phase	0.615	0.009	0.379	0.013	0.620	0.380
	0.512	0.003	0.481	0.003	0.517	0.482
	0.384	0.003	0.610	0.003	0.388	0.612
	0.281	0.024	0.713	0.026	0.283	0.716
	0.162	0.003	0.830	0.003	0.165	0.834
	x, CO	s, CO	x, CO_2	s, CO_2	x, CO (HYSYS)	x, CO_2 (HYSYS)
Liquid Phase	0.062	0.001	0.251	0.010	0.058	0.270
	0.053	0.002	0.379	0.005	0.050	0.337
	0.042	0.002	0.440	0.006	0.040	0.422
	0.033	0.001	0.536	0.009	0.031	0.490
	0.022	0.001	0.609	0.005	0.020	0.574

The binary interaction parameters used in the simulations are shown in Table 3.26.

Table 3.26: Binary interaction parameters used in the PR EoS

Compounds		T (°C)	k_{ij}	Comments
CO_2	CO	40	0.21	use as reported [Lopez-Castillo et al., 2006]
		60	0.27	extrapolated from kij values fit to literature data [Christiansen et al., 1974; Lopez-Castillo et al., 2006]
CO_2	nonanal	40	0.035	from model fit of binary VLE data from this work
		60	0.03	from model fit of binary VLE data from this work
CO	nonanal	40	0.07	from model fit of binary VLE data from this work
		60	0.09	from model fit of binary VLE data from this work

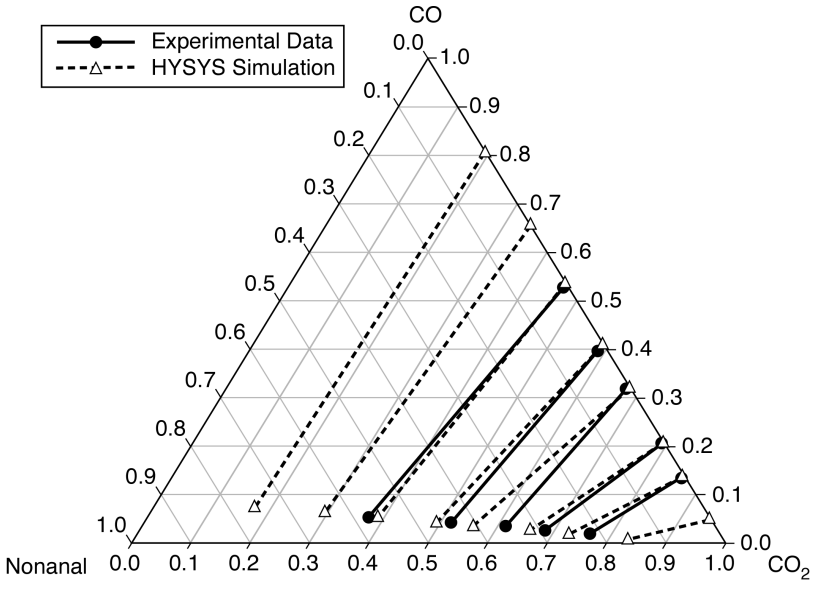

Figure 3.11: VLE of CO/CO_2/nonanal at 40 ^oC and 8 MPa

The experimental and simulated VLE data for CO/CO_2/nonanal system at 40 and 60 ^oC at 8 MPa are compared in Figure 3.11 and 3.12, respectively.

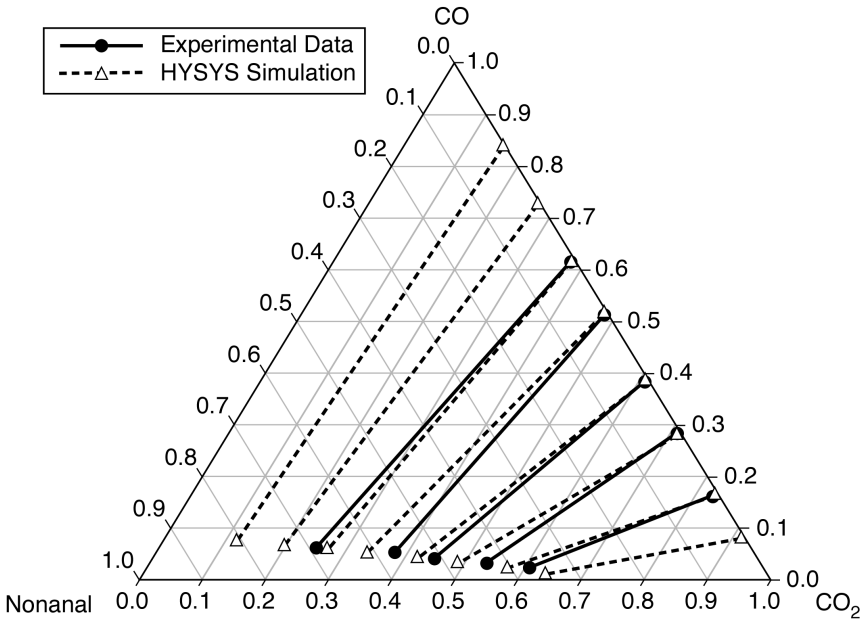

Figure 3.12: VLE of CO/CO_2/nonanal at 60 ^oC and 8 MPa

Tables 3.27 and 3.28 summarize the EF for CO solubility in CO_2-expanded nonanal relative to that in neat nonanal at identical temperature and gas phase CO fugacities.

Table 3.27: CO solubility in neat and CXL-nonanal (40 ^oC, total pressure 8 MPa)

f_{CO}, MPa	x, CO_2 (CXL)	x, CO (CXL)	x, CO (pure)	EF
1.08	0.762	0.021	0.014	1.51
1.65	0.684	0.027	0.020	1.33
2.55	0.613	0.037	0.030	1.21
3.17	0.517	0.043	0.037	1.16
4.23	0.374	0.054	0.049	1.10

Table 3.28: CO solubility in neat and CXL-nonanal (60 ^{o}C, total pressure 8 MPa)

f_{CO}, MPa	x, CO_2 (CXL)	x, CO (CXL)	x, CO (pure)	EF
1.28	0.565	0.022	0.017	1.35
2.22	0.482	0.033	0.027	1.24
3.03	0.447	0.042	0.035	1.20
4.07	0.371	0.053	0.046	1.16
4.88	0.251	0.062	0.055	1.12

Table 3.29: %AARD for HYSYS Modeling using Peng-Robinson EoS

CO(1)/CO_2(2)/Nonanal(3)	%AARD		
	x_1	x_2	x_3
40 °C	5.55	6.43	7.34
60 °C	8.88	9.24	8.87

EF values exceeding 1 are obtained for all conditions studied. At constant total pressure, the EF values increase with increasing CO_2 content in the liquid phase. The dissolved CO_2 serves to increases the free volume in the CXL phase, enhancing the CO solubility.

Table 3.29 summarizes the fit between experimental and simulated VLE data using %AARD in the CO mole fractions in the liquid phase. In general, the experimental and simulated results show reasonable good agreement considering that only binary interaction parameters were used. The simulated results for nonanal-based systems are not as good as 1-octene systems presumably because the Peng-Robinson EoS works better for non-polar or slightly polar solvents. The polarity of nonanal is significantly higher than 1-octene.

3.4 Solubilities of H_2 in Neat and CO_2-Expanded Solvents

3.4.1 VLE of H_2/1-Octene Binary Systems

Figure 3.13 shows the VLE of H_2/1-octene mixtures were measured at 40 and 60 ^oC and at pressures between 1 and 8 MPa. The experimental errors are within the size range of the data points. In general, while the H_2 solubility increased with total pressure, the temperature had a relatively weak effect on H_2 solubility.

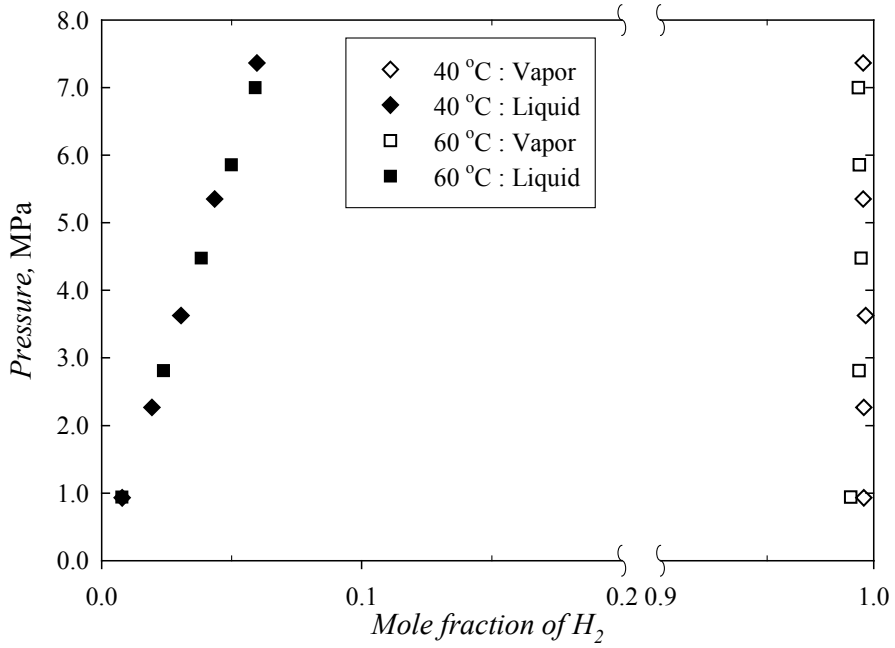

Figure 3.13: VLE of H_2/1-octene at 40 ^oC and 60 ^oC

The VLE data of H_2/1-octene binary system at 40 ^oC and 60 ^oC are summarized in Tables 3.30 and 3.31, respectively.

Table 3.30: VLE data of H_2/1-octene at 40 ^oC

P, MPa	x, H_2	x, 1-Octene	s	y, H_2	y, 1-Octene	s
0.93	0.008	0.992	0.0001	0.995	0.005	0.001
2.27	0.019	0.981	0.0001	0.995	0.005	0.001
3.63	0.031	0.969	0.0010	0.996	0.004	0.001
5.35	0.043	0.957	0.0034	0.995	0.005	0.001
7.36	0.060	0.940	0.0060	0.995	0.005	0.001

Table 3.31: VLE data of H_2/1-octene at 60 ^oC

P, MPa	x, H_2	x, 1-Octene	s	y, H_2	y, 1-Octene	s
0.94	0.008	0.992	0.000	0.989	0.011	0.001
2.81	0.024	0.976	0.001	0.993	0.007	0.001
4.48	0.038	0.962	0.001	0.994	0.006	0.002
5.86	0.050	0.950	0.002	0.993	0.007	0.001
7.00	0.059	0.941	0.001	0.993	0.007	0.001

Table 3.32 compares the estimated Henry's law constants with those reported in the literature (Peramanu and Pruden [1997], Purwanto et al [1996], Jin [2006] and Jauredui-Haza et al [2004]).

The results obtained in this study are in excellent agreement with the value reported by Jin at 60 ^oC. The constants fall in the general range of reported values although the values reported by Jauredui-Haza et al. at higher temperatures are similar to values reported at lower temperatures.

Table 3.32: Henry's law constants for H_2 in 1-octene at various temperatures

T, K	10^{-5} *K_H, Mpa	Reference
295	166	Peramanu and Pruden [1997]
298	156	Purwanto et al. [1996]
313	125	This work
323	135	Purwanto et al. [1996]
333	118	This work
333	116	Jin, H. [2006]
353	137	Jauredui-Haza et al. [2004]
363	135	Jauredui-Haza et al. [2004]
373	133	Jauredui-Haza et al. [2004]

3.4.2 VLE of H_2/CO_2/1-Octene Ternary Systems

The VLE data of H_2/CO_2/1-octene at 40, 60 ^oC and pressure 8 MPa were studies (Table 3.33, 3.34). The data in each row of the tables represent a tie line in a ternary diagram. Several different tie lines were obtained at a given pressure. The mole fractions of H_2, CO_2 and 1-octene in each phase add up to 1. For clarity, only the CO_2 and H_2 mole fractions are shown in the tables, with the balance being nonanal. The standard deviations (s) associated with the measurements and the VLE data simulated using HYSYS® are also included in Tables 3.33 and 3.34.

The binary interaction parameters used for this study as well as their source was shown in Table 3.35.

Table 3.33: VLE data of H_2/CO_2/1-octene at 40 ^oC and 8 MPa

	y, H_2	s, H_2	y, CO_2	s, CO_2	y, H_2 (HYSYS)	y, CO_2 (HYSYS)
Vapor Phase	0.762	0.006	0.231	0.002	0.762	0.237
	0.557	0.002	0.437	0.002	0.558	0.438
	0.374	0.003	0.621	0.004	0.375	0.622
	0.253	0.004	0.743	0.004	0.253	0.743
	0.157	0.004	0.838	0.004	0.157	0.838
	x, H_2	s, H_2	x, CO_2	s, CO_2	x, H_2 (HYSYS)	x, CO_2 (HYSYS)
Liquid Phase	0.051	0.001	0.209	0.008	0.051	0.198
	0.040	0.002	0.373	0.010	0.041	0.350
	0.030	0.001	0.519	0.002	0.031	0.491
	0.023	0.001	0.607	0.009	0.024	0.596
	0.017	0.002	0.728	0.010	0.018	0.695

Table 3.34: VLE data of H_2/CO_2/1-octene at 60 ^oC and 8 MPa

	y, H_2	s, H_2	y, CO_2	s, CO_2	y, H_2 (HYSYS)	y, CO_2 (HYSYS)
Vapor Phase	0.463	0.004	0.531	0.005	0.464	0.531
	0.365	0.015	0.629	0.002	0.365	0.629
	0.241	0.001	0.754	0.004	0.240	0.752
	0.184	0.002	0.812	0.004	0.180	0.812
	0.710	0.004	0.281	0.004	0.715	0.282
	x, H_2	s, H_2	x, CO_2	s, CO_2	x, H_2 (HYSYS)	x, CO_2 (HYSYS)
Liquid Phase	0.036	0.001	0.363	0.005	0.036	0.344
	0.030	0.000	0.424	0.007	0.030	0.407
	0.022	0.001	0.497	0.011	0.022	0.490
	0.018	0.001	0.553	0.003	0.018	0.534
	0.049	0.001	0.202	0.007	0.049	0.190

Table 3.35: Binary interaction parameters used in the PR EoS

Compounds		T (°C)	k_{ij}	Comments
CO_2	H_2	40	0.31	use as reported [Lopez-Castillo et al., 2008]
				extrapolated from kij values fit to literature
		60	0.4	data[Bezanehtak et al., 2004; Lopez-Castillo et al., 2008]
H_2	1-octene	40	0.1	from model fit of binary VLE data from this work
		60	0.2	from model fit of binary VLE data from this work
CO_2	1-octene	40	0.08	from model fit of binary VLE data from this work
		60	0.09	from model fit of binary VLE data from this work

The experimental and simulated VLE data for H_2/CO_2/1-octene system at 40 and 60 ^oC at 8 MPa are compared in Figure 3.14 and 3.15, respectively.

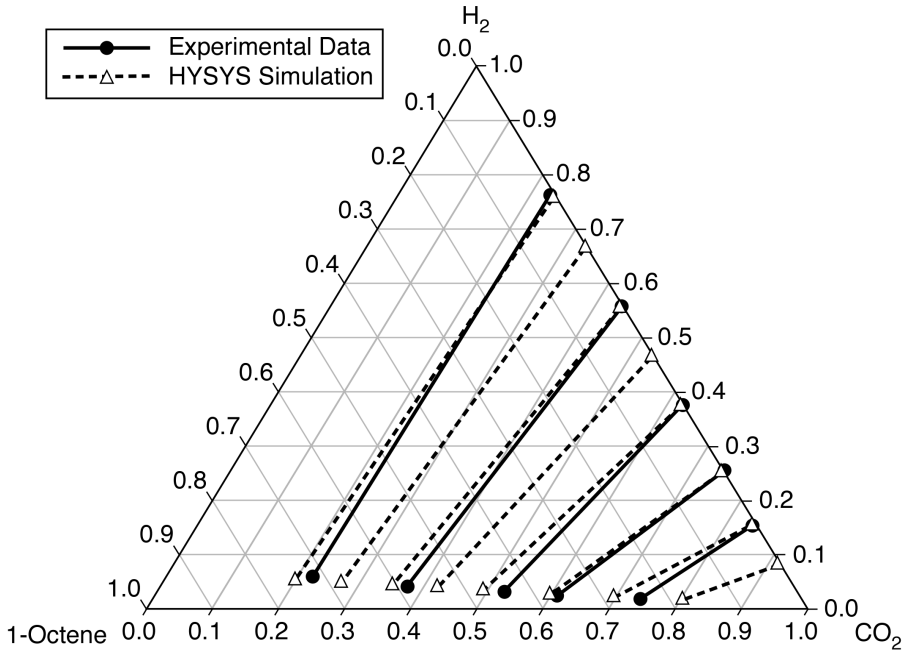

Figure 3.14: VLE of H_2/CO_2/1-octene at 40 ^oC and 8 MPa

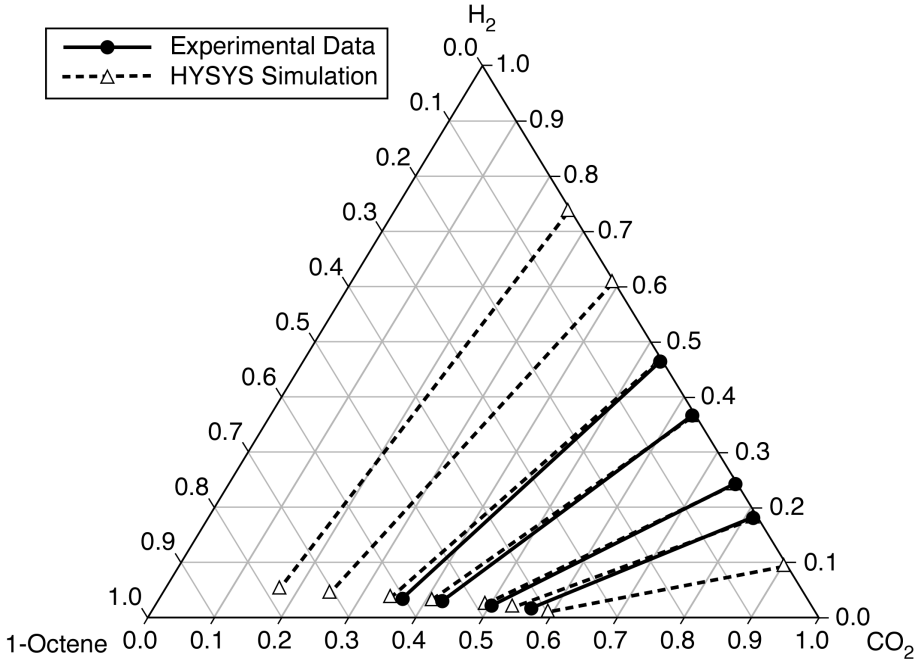

Figure 3.15: VLE of H_2/CO_2/1-octene at 60 ^oC and 8 MPa

Tables 3.36 and 3.37 summarize the Enhancement Factor (EF) for H_2 solubility in CO_2-expanded 1-octene relative to that in neat 1-octene at identical temperature and gas phase H_2 fugacities.

Table 3.36: H_2 solubility in neat and CXL-octene (40 ^oC, total pressure 8 MPa)

f_{H2}, MPa	x, CO_2 (CXL)	x, H_2 (CXL)	x, H_2 (Pure)	EF
1.29	0.736	0.017	0.011	1.62
2.07	0.607	0.023	0.017	1.36
3.07	0.524	0.030	0.025	1.20
4.57	0.373	0.040	0.037	1.08
6.25	0.222	0.051	0.050	1.01

Table 3.37: H_2 solubility in neat and CXL-octene (60 ^oC, total pressure 8 MPa)

f_{H2}, MPa	x, CO_2 (CXL)	x, H_2 (CXL)	x, H_2 (Pure)	EF
1.51	0.553	0.018	0.013	1.41
1.97	0.497	0.022	0.017	1.32
2.99	0.424	0.030	0.025	1.19
3.80	0.363	0.036	0.032	1.11
5.82	0.202	0.049	0.049	1.01

EF values exceeding 1 are obtained for all conditions studied. At constant total pressure, the EF values increase with increasing CO_2 content in the liquid phase. The dissolved CO_2 serves to increases the free volume in the CXL phase, enhancing the H_2 solubility.

Table 3.38 summarizes the fit between experimental and simulated VLE data using the percent absolute average deviations (%AARD) in the H_2 mole fractions in the liquid phase. In general, the experimental and simulated results show reasonable good agreement considering that only binary interaction parameters were used.

Table 3.38: %AARD for HYSYS Modeling using Peng-Robinson EoS

$H_2(1)/CO_2(2)$/1-Octene(3)	%AARD		
	x_1	x_2	x_3
40 °C	3.98	5.78	6.60
60 °C	1.58	4.00	2.68

3.4.3 VLE of H_2/Nonanal Binary Systems

Figure 3.13 shows the VLE of H_2/nonanal mixtures were measured at 40 and 60 ^oC and at pressures between 1 and 8 MPa. The experimental errors are within the size

range of the data points. In general, while the H_2 solubility increased with total pressure, the temperature had a relatively weak effect on H_2 solubility.

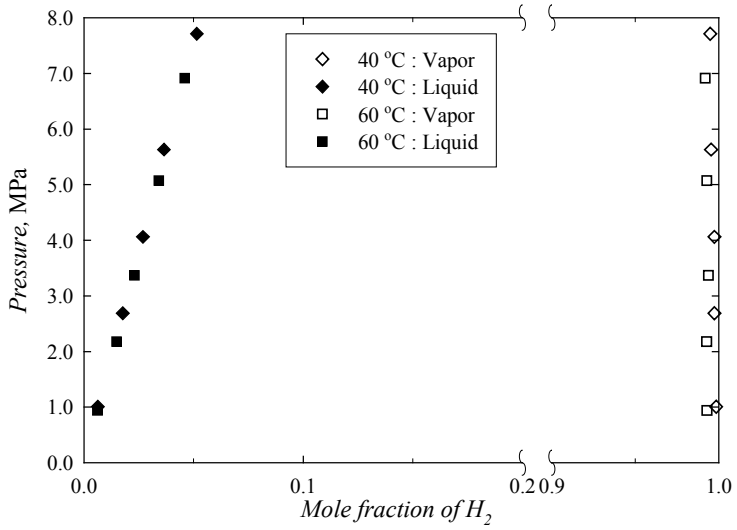

Figure 3.16: VLE of H_2/nonanal at 40 °C and 60 °C

The VLE data of H_2/nonanal binary system at 40 °C and 60 °C are summarized in Tables 3.39 and 3.40, respectively.

Table 3.39: VLE data of H_2/nonanal at 40 °C

P, MPa	x, H_2	x, Nonanal	s	y, H_2	y, Nonanal	s
1.01	0.006	0.994	0.0001	0.999	0.001	0.001
2.69	0.018	0.982	0.0004	0.997	0.003	0.002
4.06	0.027	0.973	0.0007	0.998	0.002	0.002
5.63	0.037	0.963	0.0010	0.995	0.005	0.001
7.71	0.052	0.948	0.0016	0.995	0.005	0.001

Table 3.40: VLE data of H_2/nonanal at 60 ^oC

P, MPa	x, H_2	x, Nonanal	s	y, H_2	y, Nonanal	s
0.94	0.006	0.994	0.0001	0.993	0.007	0.0005
2.18	0.015	0.985	0.0002	0.993	0.007	0.0012
3.37	0.023	0.977	0.0012	0.994	0.006	0.0002
5.07	0.034	0.966	0.0009	0.993	0.007	0.0006
6.91	0.046	0.954	0.0003	0.992	0.008	0.0000

Table 3.41 compares the estimated Henry's law constants with those reported in the literature data of Jauredui-Haza et al [2004].

Table 3.41: Henry's law constants for H_2 in nonanal at various temperatures

T, K	$10^{-5}*K_H$, MPa^{-1}	Reference
313	164	This work
333	161	
353	225	
363	216	Jauredui-Haza et al.[2004]
373	211	

3.4.4 VLE of H_2/CO_2/Nonanal Ternary Systems

The VLE data of H_2/CO_2/nonanal at 40, 60 ^oC and pressure 8 MPa were studies (Table 3.42, 3.43). The data in each row of the tables represent a tie line in a ternary diagram. Several different tie lines were obtained at a given pressure. The mole fractions of H_2, CO_2 and nonanal in each phase add up to 1. For clarity, only the CO_2 and H_2 mole fractions are shown in the tables, with the balance being nonanal. The standard deviations (s) associated with the measurements and the VLE data simulated

using HYSYS® are also included in Tables 3.42 and 3.43. The binary interaction parameters used for this study as well as their source was shown in Table 3.44. The experimental and simulated VLE data for H_2/CO_2/nonanal system at 40 and 60 ^oC at 8 MPa are compared in Figure 3.17 and 3.18, respectively.

Table 3.42: VLE data of H_2/CO_2/nonanal at 40 ^oC and 8 MPa

	y, H_2	s, H_2	y, CO_2	s, CO_2	y, H_2 (HYSYS)	y, CO_2 (HYSYS)
Vapor Phase	0.837	0.002	0.153	0.002	0.847	0.153
	0.562	0.005	0.431	0.002	0.568	0.432
	0.438	0.003	0.556	0.004	0.443	0.557
	0.312	0.004	0.682	0.004	0.316	0.684
	0.183	0.004	0.811	0.004	0.186	0.813
	x, H_2	s, H_2	x, CO_2	s, CO_2	x, H_2 (HYSYS)	x, CO_2 (HYSYS)
Liquid Phase	0.046	0.003	0.163	0.008	0.045	0.150
	0.035	0.002	0.419	0.010	0.033	0.383
	0.029	0.001	0.510	0.002	0.028	0.479
	0.024	0.001	0.592	0.009	0.022	0.577
	0.018	0.002	0.715	0.010	0.015	0.686

Table 3.43: VLE data of H_2/CO_2/nonanal at 60 ^oC and 8 MPa

	y, H_2	s, H_2	y, CO_2	s, CO_2	y, H_2 (HYSYS)	y, CO_2 (HYSYS)
Vapor Phase	0.775	0.004	0.220	0.005	0.780	0.220
	0.615	0.015	0.379	0.002	0.620	0.380
	0.442	0.001	0.551	0.004	0.447	0.553
	0.262	0.002	0.732	0.004	0.265	0.735
	0.130	0.004	0.863	0.004	0.132	0.868
	x, H_2	s, H_2	x, CO_2	s, CO_2	x, H_2 (HYSYS)	x, CO_2 (HYSYS)
Liquid Phase	0.044	0.001	0.190	0.005	0.042	0.171
	0.037	0.000	0.297	0.007	0.035	0.280
	0.028	0.001	0.439	0.011	0.026	0.412
	0.020	0.001	0.553	0.003	0.018	0.508
	0.013	0.001	0.617	0.007	0.012	0.591

Table 3.44: Binary interaction parameters used in the PR EoS

Compounds		T (^oC)	k_{ij}	Comments
CO_2	H_2	40	0.31	use as reported[1]
		60	0.4	extrapolated from kij values fit to literature data[1,2]
H_2	nonanal	40	0.07	from model fit of binary VLE data from this work
		60	0.10	from model fit of binary VLE data from this work
CO_2	nonanal	40	0.035	from model fit of binary VLE data from this work
		60	0.03	from model fit of binary VLE data from this work

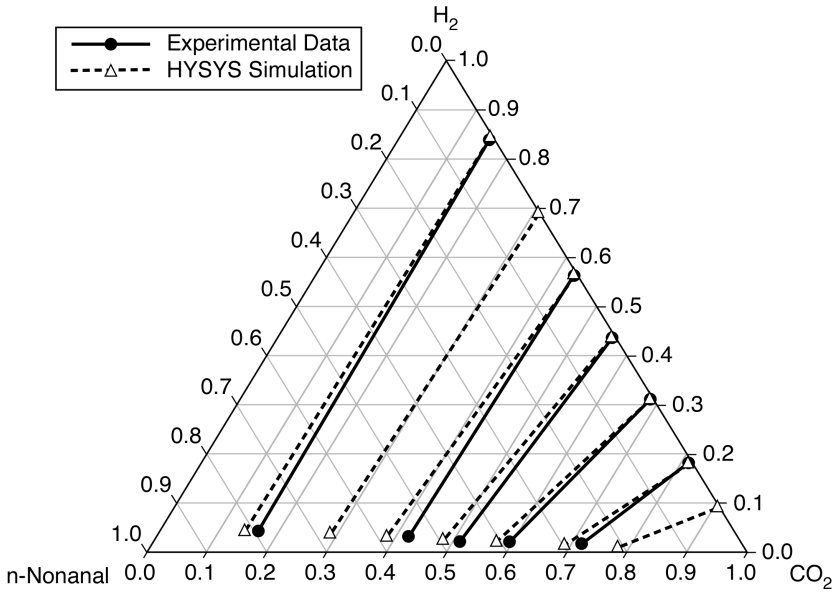

Figure 3.17: VLE of H_2/CO_2/nonanal at 40 ^oC and 8 MPa

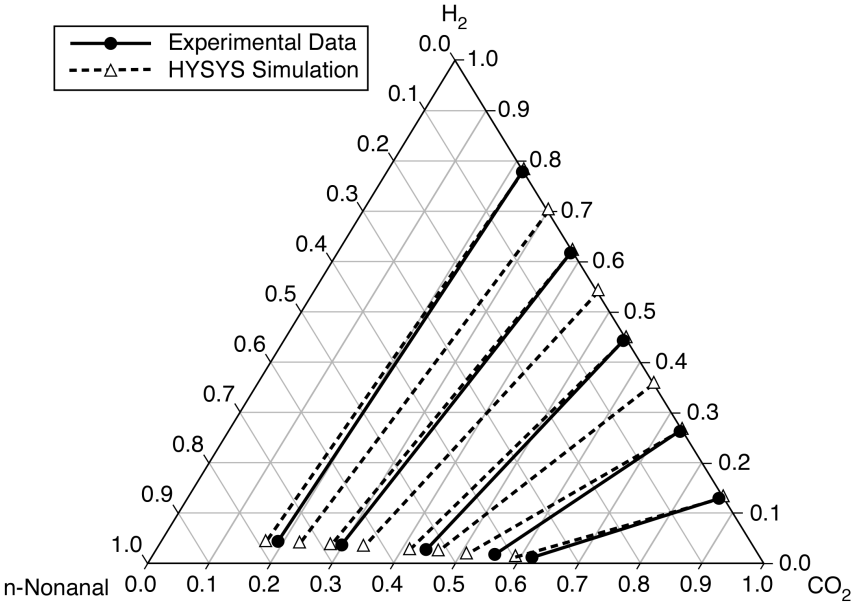

Figure 3.18: VLE of H_2/CO_2/nonanal at 60 ^oC and 8 MPa

Tables 3.45 and 3.46 summarize the Enhancement Factor (EF) for H_2 solubility in CO_2-expanded nonanal relative to that in neat nonanal at identical temperature and

gas phase H_2 fugacities.

Table 3.45: H_2 solubility in neat and CXL-nonanal (40 ^oC, total pressure 8 MPa)

f_{H2}, MPa	x, CO_2 (CXL)	x, H_2 (CXL)	x, H_2 (Pure)	EF
1.50	0.715	0.018	0.010	1.82
2.56	0.592	0.024	0.017	1.40
3.59	0.510	0.029	0.023	1.24
4.61	0.419	0.035	0.030	1.15
6.86	0.163	0.046	0.044	1.04

Table 3.46: H_2 solubility in neat and CXL-nonanal (60 ^oC, total pressure 8 MPa)

f_{H2}, MPa	x, CO_2 (CXL)	x, H_2 (CXL)	x, H_2 (Pure)	EF
1.07	0.617	0.013	0.007	1.76
2.15	0.553	0.020	0.014	1.36
3.62	0.472	0.028	0.024	1.17
5.04	0.297	0.037	0.033	1.10
6.36	0.190	0.044	0.042	1.05

EF values exceeding 1 are obtained for all conditions studied. At constant total pressure, the EF values increase with increasing CO_2 content in the liquid phase. The dissolved CO_2 serves to increases the free volume in the CXL phase, enhancing the H_2 solubility.

Table 3.47 summarizes the fit between experimental and simulated VLE data using the percent absolute average deviations (%AARD) in the H_2 mole fractions in the liquid phase. In general, the experimental and simulated results show reasonable good agreement considering that only binary interaction parameters were used. Again,

the simulated results for nonanal-based systems are not as good as 1-octene systems presumably because the Peng-Robinson EoS works better for non-polar or slightly polar solvents.

Table 3.47: %AARD for HYSYS Modeling using Peng-Robinson EoS

$H_2(1)/CO_2(2)$/Nonanal(3)	%AARD		
	x_1	x_2	x_3
40 ^oC	8.48	7.39	8.00
60 ^oC	6.49	6.72	5.78

CHAPTER 4 CONCLUSIONS AND RECOMMENDATIONS

4.1 Conclusions

In this thesis, the vapor liquid equilibria of the following binary and ternary systems were measured in a variable volume view cell at temperatures ranging from 40-80°C and pressures up to 9 MPa: CO/1-octene, CO_2/1-octene, CO/1-octene/CO_2, CO/nonanal, CO_2/nonanal CO/nonanal/CO_2, H_2/1-octene, H_2/1-octene/CO_2, H_2/nonanal and H_2/nonanal/CO_2. The vapor and liquid phases at equilibrium were sampled at constant pressure and analyzed using a gas chromatograph.

The VLE data for the CO/1-octene and CO_2/1-octene systems were measured at 40, 60 and 80 ^oC respectively and at pressures between 1 and 9 MPa. The VLE data for the CO/nonanal, CO_2/nonanal, H_2/1-octene, H_2/nonanal binary systems were measured at 40 and 60 ^oC respectively and at pressures between 1 and 8 MPa. The solubilities of CO, H_2 and CO_2 in the solvents followed Henry's law and were consistent with literature values. The gas solubilities in the liquid phase increased linearly with an increase in gas phase fugacity of the pure component. Temperature has virtually has no effect on the solubility of CO or H_2 in the solvents in the range of operating conditions investigated. An increase of temperature reduced the solubility of CO_2 in the solvents.

The VLE data for the CO/1-octene/CO_2, CO/nonanal/CO_2, H_2/1-octene/CO_2 and H_2/nonanal/CO_2 ternary systems was measured at temperatures ranging from 40-80°C and 8 MPa. In all cases, an increase of CO_2 content in the liquid phase enhances the solubilities of both CO and H_2 in the liquid phase. The enhancement factor (EF),

defined as the ratio of the equilibrium gas solubility in the CO_2-expanded liquid relative to that in the neat liquid at a fixed gas phase fugacity, is up to 1.82 for hydrogen and 1.54 for carbon monoxide. EF values greater than 1 are obtained for all conditions studied. At constant pressure, EF increases with the increase of CO_2 in the liquid phase. This increase is attributed to the increase in free volume in the CO_2-expanded liquid phase which favors syngas solubility. The enhancements of syngas solubility are higher in product mixtures (CXL-nonanal) than in reactant mixtures (CXL-octene).

Aspen HYSYS software was used to simulate the ternary phase equilibrium using Peng-Robinson equation of state (PR EoS) with van der Waals mixing rules and binary interaction parameters. PR EoS modeled the VLE data adequately, with much better fits for the 1-octene systems compared to the more polar nonanal systems.

4.2 Recommendations

The results of this thesis pave the way for several follow-up studies as listed below:

1. Measurements of the solubilities of H_2 and CO in mixtures of 1-octene and nonanal to investigate the effect of product formation on gas solubility.
2. Expand reaction systems to a broader and more practical range of substrates, such as the mixed-olefin and the branched-olefin feeds used in industrial oxo processes, as well as the starting materials used in specialty and asymmetric hydroformylation processes.
3. Attempt different equations of state or activity coefficient models (such as

Soave-Redlich-Kwong, UNIQUAC) for simulating the ternary phase equilibria.

4. Use HYSYS with appropriate equation of state to predict vapor-liquid equilibrium of systems under wider range of temperatures and pressures.
5. Measure vapor-liquid equilibrium data with the presence of catalysts.

REFERENCES

Bezanehtak, K., F. Dehghani, et al. Vapor-Liquid Equilibrium for the Carbon Dioxide + Hydrogen + Methanol Ternary System. *J. Chem. Eng. Data*, 49(3): 430-434, (2004).

Bonate, P. L. Concepts in calibration theory, part III: weighted least-squares regression. . *LC-GC*, 10(6): 448-50, (1992).

Bonate, P. L. Concepts in calibration theory. Part II: regression through the origin - when should it be used? *LC-GC*, 10(5): 378-9, (1992).

Bonate, P. L. Concepts in calibration theory. Part I: regression. *LC-GC*, 10(4) (1992).

Bonate, P. L. Concepts in calibration theory. Part IV. Prediction and confidence intervals. *LC-GC*, 10(7) (1992).

Brunner, E. Solubility of hydrogen in 10 organic solvents at 298.15, 323.15, and 373.15 K. *J. Chem. Eng. Data*, 30(3): 269-273, (1985).

Christiansen, L. J., A. Fredenslund, et al. Gas-liquid equilibriums carbon dioxide-carbon monoxide and carbon dioxide-methane-carbon monoxide systems. *Advances in Cryogenic Engineering* 19: 309-319, (1974).

Christov, M. and R. Dohrn. High-pressure fluid phase equilibria: Experimental methods and systems investigated (1994-1999). *Fluid Phase Equilibria*, 202(1): 153-218, (2002).

Clevett, K. J. Process analyzer technology. New York, Wiley, (1986).

Cornils, B. and W. A. Herrmann, Eds. Applied homogeneous catalysis with organometallic compounds : a comprehensive handbook in three volumes. Weinheim, Wiley-VCH, (2002).

Day, C.-Y. Phase Equilibrium of Ethanol + CO_2 and Acetone + CO_2 at Elevated Pressures. *Journal of chemical and engineering data*, 41(4): 839-843, (1996).

Deschamps, J., D. H. Menz, et al. Low pressure solubility and thermodynamics of solvation of oxygen, carbon dioxide, and carbon monoxide in fluorinated liquids. *The Journal of Chemical Thermodynamics*, 39(6): 847-854, (2007).

Dohrn, R., B. v. Phasengleichgewichten, et al. (1994).

Guha, D., H. Jin, et al. Mass Transfer Effects during Homogeneous 1-Octene Hydroformylation in CO2-expanded Solvent: Modeling and Experiments. *Chemical Engineering Science*, 62: 4967-4975, (2007).

Heldebrant, D. J., H. N. Witt, et al. Liquid polymers as solvents for catalytic reductions. *Green Chem.*, 8: 807 - 815, (2006).

Hert, D. G., J. L. Anderson, et al. Enhancement of oxygen and methane solubility in 1-hexyl-3-methylimidazolium bis(trifluoromethylsulfonyl) imide using carbon dioxide. *Chemical Communications*, 20: 2603-2605, (2005).

Houndonougbo, Y., H. Jin, et al. Phase Equilibria in Carbon Dioxide Expanded

Solvents: Experiment and Molecular Simulations. *J. Physical Chemistry B.*, 110(26): 13195-13202, (2006).

Houndonougbo, Y., K. Kuczera, et al. Prediction of the Phase Equilibria and Transport Properties in Carbon-Dioxide Expanded Solvents by Molecular Simulation. *Molecular Simulation*, 33(9): 861-869, (2007).

Jacquemin, J., M. F. Costa Gomes, et al. Solubility of carbon dioxide, ethane, methane, oxygen, nitrogen, hydrogen, argon, and carbon monoxide in 1-butyl-3-methylimidazolium tetrafluoroborate between temperatures 283K and 343K and at pressures close to atmospheric. *The Journal of Chemical Thermodynamics*, 38(4): 490-502, (2006).

Jáuregui-Haza, U. J., E. J. Pardillo-Fontdevila, et al. Solubility of hidrogen and carbon monoxide in water and some organic solvents. *Latin American Applied Research*, 34(2): 71-74, (2004).

Jessop, P. G. and B. Subramaniam. Gas-Expanded Liquids. *Chem. Rev.*, 107(6): 2666-2694, (2007).

Jin, H. Exploiting carbon dioxide-expanded as reaction media for catalytic hydroformylation of higher olefins. Lawrence, University of Kansas. PhD 2006.

Jin, H., B. Subramaniam, et al. Intensification of catalytic olefin hydroformylation in CO_2-expanded media. *AIChE Journal*, 52(7): 2575-2581, (2006).

Kaminishi, G. and T. Toriumi. Vapor-liquid equilibria in the systems: carbon dioxide-carbon monoxide, carbon dioxide-carbon monoxide-hydrogen, carbon dioxide-methane. *Review of Physical Chemistry of Japan* 38(1): 79-84, (1968).

Katayama, T., K. Ohgaki, et al. Isothermal vapor-liquid equilibriums of acetone-carbon dioxide and methanol-carbon dioxide systems at high pressures. *Journal of Chemical Engineering of Japan* 8(2): 89-92, (1975).

Kumelan, J., A. Perez-Salado Kamps, et al. Solubility of the single gases H_2 and CO in the ionic liquid [bmim][CH_3SO_4]. *Fluid Phase Equilibria*, 260(1): 3-8, (2007).

Leeuwen, P. W. N. M. v. and C. Claver. Rhodium catalyzed hydroformylation. Dordrecht [Netherlands] ; Boston, Kluwer Academic Publishers, (2000).

Lopez-Castillo, Z. K., S. N. V. K. Aki, et al. Enhanced Solubility of Oxygen and Carbon Monoxide in CO_2-Expanded Liquids. *Ind. Eng. Chem. Res.*, 45(15): 5351-5360, (2006).

Lopez-Castillo, Z. K., S. N. V. K. Aki, et al. Enhanced Solubility of Hydrogen in CO_2-Expanded Liquids. *Ind. Eng. Chem. Res.*, 47(3): 570-576, (2008).

McNair, H. M. and J. M. Miller. Basic gas chromatography. New York, Wiley, (1998).

Mickley, H. S. Applied mathematics in chemical engineering. New York,, McGraw-Hill, (1957).

Neter, J. and W. Wasserman. Applied linear statistical models; regression, analysis of variance, and experimental designs. Homewood, Ill.,, R. D. Irwin, (1974).

Peramanu and Pruden. *Canadian Journal of Chemical Engineering*, 75(3): 535-543, (1997).

Preston, F. W. Analysis of uncertainty in experimental measurements. (Class notes). Lawrence, Kansas, University of Kansas 1986.

Purwanto, R. M. Deshpande, et al. Solubility of Hydrogen, Carbon Monoxide, and 1-Octene in Various Solvents and Solvent Mixtures. *J. Chem. Eng. Data*, 41(6): 1414-1417, (1996).

Roelen, O. Production of oxygenated carbon compounds. G. Patent 1938/1952.

Shaharun, M. S., H. Mukhtar, et al. Solubility of carbon monoxide and hydrogen in propylene carbonate and thermomorphic multicomponent hydroformylation solvent. *Chemical Engineering Science*, 63(11): 3024-3035, (2008).

Snavely, W. K. On-line gas chromatography of Fischer-Tropsch synthesis products, University of Kansas, Chemical and Petroleum Engineering, 1996.: xix, 347 leaves, 1996.

Solinas, M., A. Pfaltz, et al. Enantioselective Hydrogenation of Imines in Ionic Liquid/Carbon Dioxide Media. *J. Am. Chem. Soc.*, 126(49): 16142-16147, (2004).

Still, C., T. Salmi, et al. Solubility of gases in a hydroformylation solvent. *Chemical*

Engineering Science, 61(11): 3698-3704, (2006).

Subramaniam, B., J. A. Tunge, et al. Tuning Product Selectivity In Catalytic Hydroformylation Reactions With CO2-Expanded Liquids. U. S. 2008.

Thompson, B. Fundamentals of gas analysis by gas chromatography. Palo Alto, Calif., Varian, (1977).

Trzeciak, A. M. and J. J. Ziółkowski. Perspectives of rhodium organometallic catalysis. Fundamental and applied aspects of hydroformylation. *Coordination Chemistry Reviews*, 190-192: 883-900, (1999).

Walpole, R. E. Probability & statistics for engineers & scientists. Upper Saddle River, NJ, Prentice Hall, (2002).

Xie, X., J. S. Brown, et al. Bubble and Dew Point Measurements of the Ternary System Carbon Dioxide + Methanol + Hydrogen at 313.2 K. *J. Chem. Eng. Data*, 50(3): 780-783, (2005).

Yin, J.-Z. and C.-S. Tan. Solubility of hydrogen in toluene for the ternary system H_2 + CO_2 + toluene from 305 to 343 K and 1.2 to 10.5 MPa. *Fluid Phase Equilibria*, 242(2): 111-117, (2006).

Zevnik, L. and J. Levec. Hydrogen solubility in CO_2-expanded 2-propanol and in propane-expanded 2-propanol determined by an acoustic sensor. *The Journal of Supercritical Fluids*, 41(3): 335-342, (2007).

APPENDIX A CALIBRATION AND ERROR CALCULATION DATA

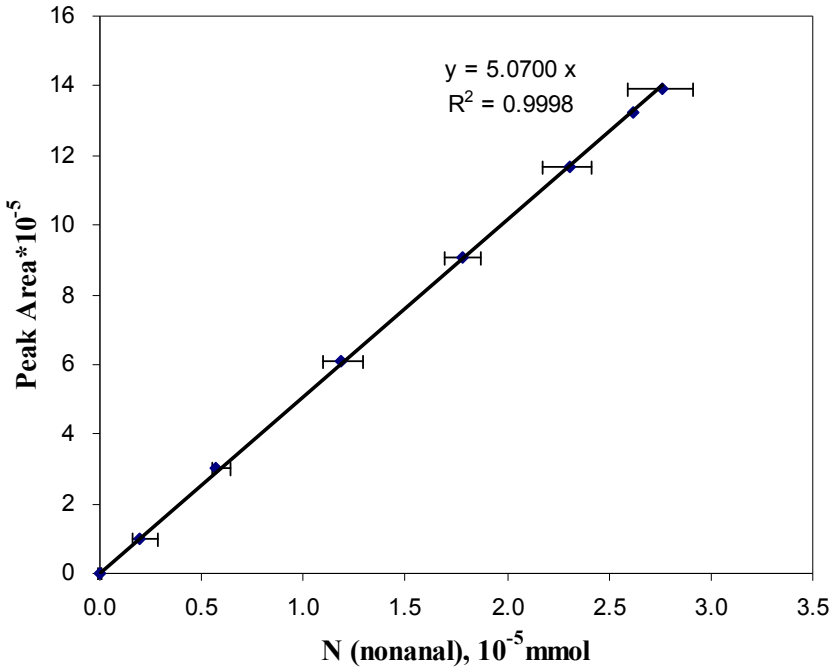

Figure A.1: Nonanal calibration curve (redraw with proper notation in the axes)

Table A.1 : Nonanal calibration data

n (nonanal), 10^{-5} mmol	PA, average	Standard Deviation	L1	L2	Error L1, %	Error L2, %
2.762	1393516	15625	2.591	2.911	6.19	5.39
2.621	1324767	11921	2.494	2.735	4.88	4.33
2.304	1168029	8866	2.217	2.392	3.76	3.84
1.779	906220	10219	1.691	1.885	4.97	5.96
1.185	612192	5140	1.160	1.255	2.06	5.94
0.573	304563	6781	0.540	0.662	5.77	15.59
0.196	99577	1300	0.185	0.208	5.74	6.15

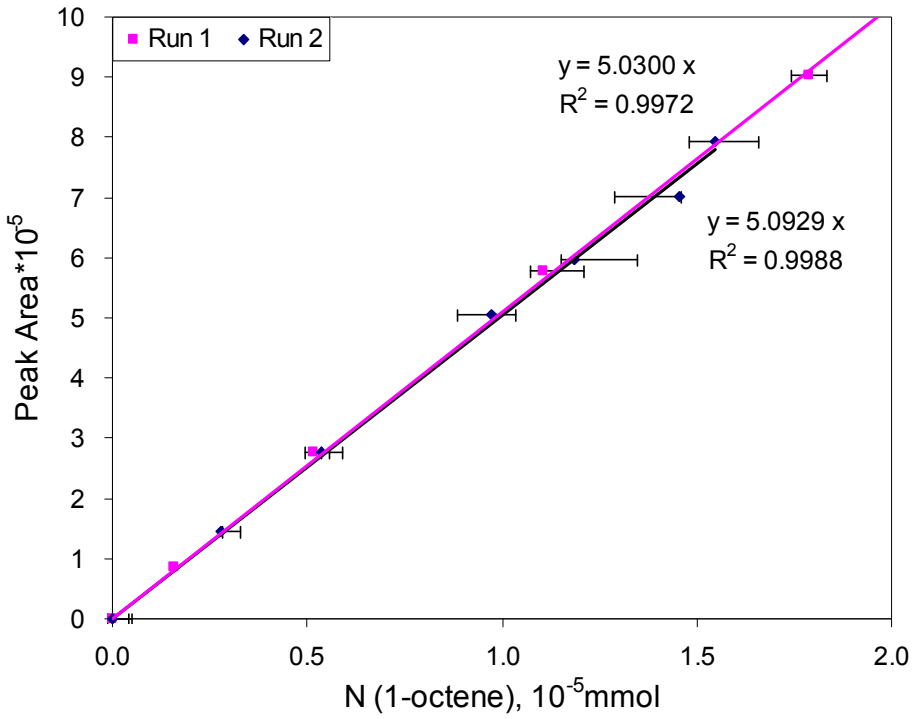

Figure A.2: 1-Octene calibration curve

Table A.2: 1-Octene calibration data (run 1)

n, 1-octene	PA, average	Standard Deviation	L1	L2	Error L1, %	Error L2, %
0.28	149741	3326	0.268	0.328	3.87	17.84
0.54	275627	3338	0.517	0.579	3.51	7.96
0.97	505303	7095	0.937	1.074	3.61	10.47
1.19	598024	4742	1.142	1.236	3.72	4.17
1.45	700748	5157	1.341	1.446	7.76	0.54
1.55	792473	7695	1.496	1.657	3.38	7.02

Table A.3: 1-Octene calibration data (run 2)

n, 1-octene	PA, average	Standard Deviation	L1	L2	Error L1, %	Error L2, %
0.16	86347	3156	0.141	0.198	10.15	25.63
0.51	276000	2618	0.518	0.565	0.71	9.82
1.11	578047	2950	1.108	1.162	0.02	4.87
1.79	903246	8104	1.698	1.850	4.93	3.58
2.49	1300141	9970	2.455	2.652	1.37	6.53
2.93	1448432	8503	2.759	2.930	5.69	0.16
3.15	1615072	18354	3.084	3.264	2.18	3.50

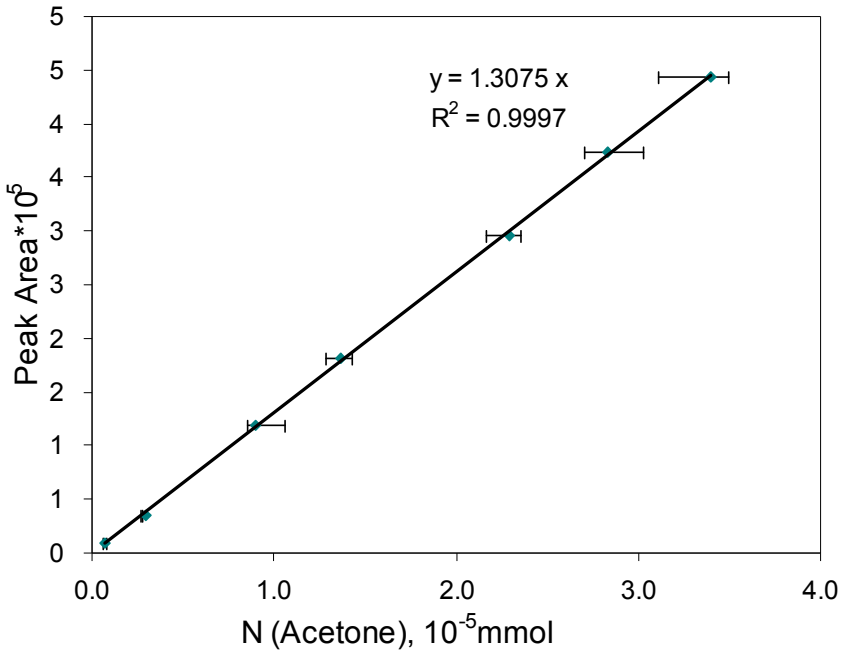

Figure A.3: Acetone calibration curve

Table A.4: Acetone calibration data

n, acetone	PA, average	Standard Deviation	L1	L2	Error L1, %	Error L2, %
3.402	443919	7123	3.108	3.498	8.64	2.82
2.829	373299	9124	2.704	3.027	4.43	6.98
2.294	295522	2394	2.170	2.351	5.38	2.51
1.370	181655	2947	1.284	1.426	6.28	4.07
0.901	118667	4385	0.854	1.063	5.27	17.95
0.294	35613	193	0.269	0.276	8.47	6.26
0.069	9323	269	0.062	0.081	10.21	16.88

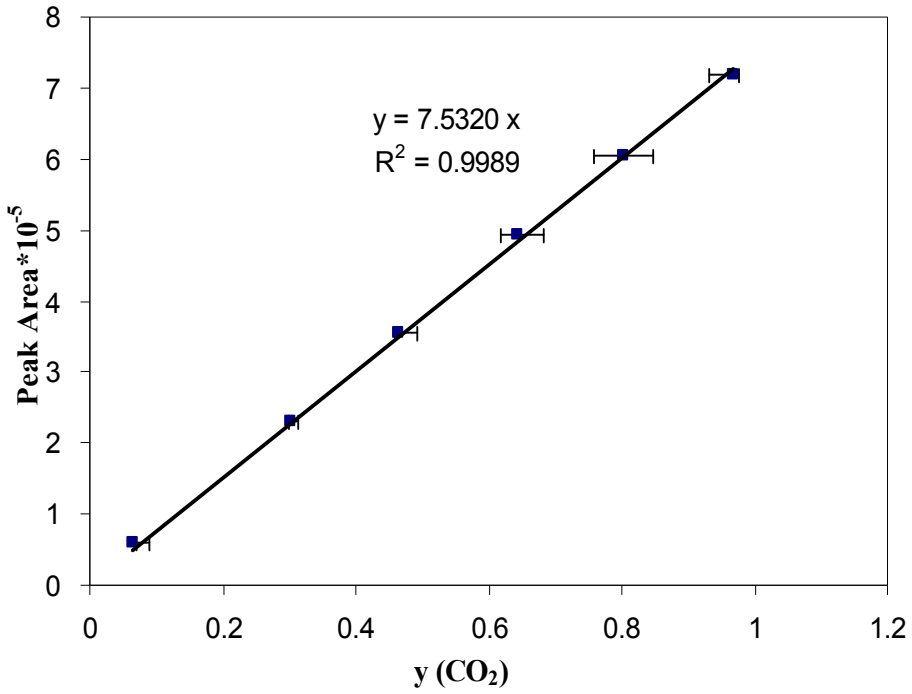

Figure A.4: CO_2 calibration curve

Table A.5: CO_2 calibration data

y, CO_2	PA, average	Standard Deviation	L1	L2	Error L1, %	Error L2, %
0.064	59317	1065	0.069	0.089	7.30	38.00
0.301	230718	778	0.299	0.314	0.83	4.04
0.465	354630	134	0.460	0.492	1.16	5.71
0.642	492734	3745	0.617	0.682	3.98	6.21
0.803	604332	4382	0.757	0.849	5.70	5.73
0.967	718515	2053	0.932	0.977	3.61	1.03

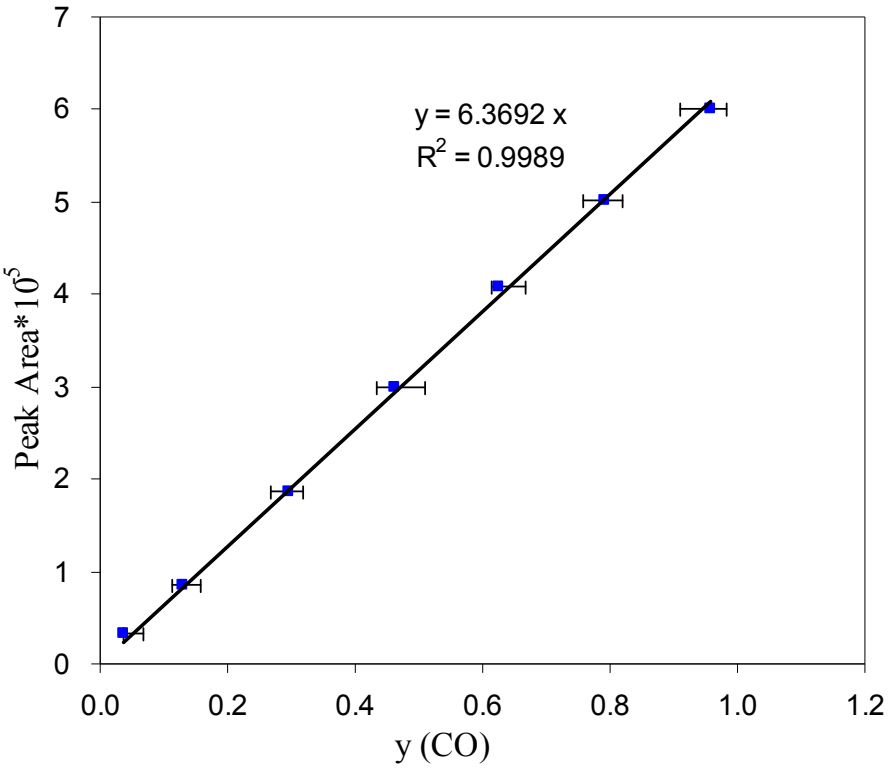

Figure A.5: CO calibration curve

Table A.6: CO calibration data

y, CO	PA, average	Standard Deviation	L1	L2	Error L1, %	Error L2, %
0.037	32796	1353	0.037	0.046	1.12	24.84
0.130	85850	2045	0.112	0.157	13.40	21.22
0.295	186623	2287	0.268	0.319	9.34	7.93
0.461	300198	3342	0.433	0.510	5.93	10.71
0.626	407832	2169	0.615	0.666	1.81	6.43
0.791	501801	2505	0.757	0.819	4.33	3.49
0.957	601781	2836	0.909	0.982	5.05	2.61